nature medicine

Article

https://doi.org/10.1038/s41591-024-02805-1

MYC targeting by OMO-103 in solid tumors: a phase 1 trial

Received: 7 February 2023

Accepted: 4 January 2024

Published online: 06 February 2024

Check for updates

Elena Garralda[1,7], Marie-Eve Beaulieu[2,7], Víctor Moreno[3], Sílvia Casacuberta-Serra[2], Sandra Martínez-Martín[2], Laia Foradada[2], Guzman Alonso[1], Daniel Massó-Vallés[2], Sergio López-Estévez[2], Toni Jauset[2], Elena Corral de la Fuente[4], Bernard Doger[3], Tatiana Hernández[3], Raquel Perez-Lopez[1], Oriol Arqués[1], Virginia Castillo Cano[2], Josefa Morales[2], Jonathan R. Whitfield[1], Manuela Niewel[2], Laura Soucek[1,2,5,6] & Emiliano Calvo[4]

Among the 'most wanted' targets in cancer therapy is the oncogene MYC, which coordinates key transcriptional programs in tumor development and maintenance. It has, however, long been considered undruggable. OMO-103 is a MYC inhibitor consisting of a 91-amino acid miniprotein. Here we present results from a phase 1 study of OMO-103 in advanced solid tumors, established to examine safety and tolerability as primary outcomes and pharmacokinetics, recommended phase 2 dose and preliminary signs of activity as secondary ones. A classical 3 + 3 design was used for dose escalation of weekly intravenous, single-agent OMO-103 administration in 21-day cycles, encompassing six dose levels (DLs). A total of 22 patients were enrolled, with treatment maintained until disease progression. The most common adverse events were grade 1 infusion-related reactions, occurring in ten patients. One dose-limiting toxicity occurred at DL5. Pharmacokinetics showed nonlinearity, with tissue saturation signs at DL5 and a terminal half-life in serum of 40 h. Of the 19 patients evaluable for response, 12 reached the predefined 9-week time point for assessment of drug antitumor activity, eight of those showing stable disease by computed tomography. One patient defined as stable disease by response evaluation criteria in solid tumors showed a 49% reduction in total tumor volume at best response. Transcriptomic analysis supported target engagement in tumor biopsies. In addition, we identified soluble factors that are potential pharmacodynamic and predictive response markers. Based on all these data, the recommended phase 2 dose was determined as DL5 (6.48 mg kg^{-1}). ClinicalTrials.gov identifier: NCT04808362.

In human cancers MYC is a frequently deregulated oncogene and a 'most wanted' target in cancer therapy[1]. It works as a pleiotropic transcription factor coordinating transcriptional programs involved in cell proliferation, cell growth, metabolism, apoptosis and immune suppression[2]. Under physiological conditions these activities are generally transient and associated with tissue regeneration programs. However, in cancer, MYC and all its corollary functions are relentlessly engaged by upstream oncogenic signals to be continuously permissive for cancer initiation

A full list of affiliations appears at the end of the paper. e-mail: Lsoucek@vhio.net

and/or maintenance[3]. It has been suggested that, under these aberrant conditions, MYC could function as a global amplifier increasing the output at all active promoters, leading to hypertranscription in cancer cells[4]. All these factors have pointed towards MYC as an excellent therapeutic target but several technical difficulties, especially the intrinsically disordered nature of the protein, have so far prevented the development of a clinically viable MYC inhibitor[1,5]. Here we report the results of a first-in-human phase 1 clinical trial to assess the safety, pharmacokinetics (PK) and preliminary signs of activity of OMO-103, a first-in-modality anti-MYC miniprotein. OMO-103 is a drug based on Omomyc, a MYC dominant negative initially designed and published in 1998 as a laboratory tool to study MYC perturbation[6,7], then later used to model MYC inhibition and its marked therapeutic potential in different mouse models of cancer, where it also showed safety and tolerability[6,8–10]. To summarize, Omomyc interferes with MYC dimerization to its obligate partner MAX and inhibits their interaction with the consensus DNA-binding site, the E-box sequence. Indeed, Omomyc sequesters MYC in protein dimers unable to bind DNA while also forming both homodimers and heterodimers with MAX, which occupy the E-boxes with transcriptionally inactive protein complexes, preventing the transcription of bona fide MYC targets[6,7,11]. Omomyc was previously expressed genetically to show that it could prevent tumorigenesis and even eradicate tumors in multiple cancer models, regardless of their driving oncogene or tissue of origin[6,8–10,12–14].

The more recent discovery of unexpected cell-penetrating properties of the purified Omomyc miniprotein led to its development as a pharmacological tool that demonstrated therapeutic efficacy both in vitro and in mouse models of non-small cell lung cancer (NSCLC)[15] and triple-negative breast cancer[16] and opened the way for its clinical development[17]. In these contexts, Omomyc showed safety and efficacy both upon intranasal and intravenous administration and induced shutdown of MYC transcriptional programs and reprogramming of the tumor microenvironment[18], recapitulating several key features of expression of the Omomyc transgene[15,16]. Its therapeutic impact was reported in both primary tumors and metastases[16], alone and in combination with standard-of-care chemotherapy (that is, paclitaxel)[15,16].

In these preclinical models, the degree of response to Omomyc correlated only with its level of expression and not with MYC levels[6,14,16].

Here we report the results of a dose-escalation phase 1 study in allcomers solid tumors, showing safety and preliminary signs of drug activity of OMO-103 under different oncological indications, supported by target engagement and immune-related biomarkers.

Results

Dose escalation and safety study

The study was carried out from May 2021 until October 2022. The first patient was enrolled on 4 May 2021 and the last on 4 April 2022; 22 patients were enrolled and treated at six DLs (1–6) (Fig. 1a,b). The patients included had a wide range of metastatic solid tumors and had received a median of four previous lines of treatment, ranging from two to 12 (see Fig. 1c for demographics). Given the lack of correlation between MYC expression and Omomyc effect in preclinical models, neither MYC amplification nor overexpression was used as an inclusion criterion but was analyzed retrospectively. Nine out of the 16 patients (56.25%) that could be evaluated showed >50% MYC^+ cells at baseline by immunohistochemistry (Extended Data Fig. 1). Only two out of 16 patients (12.5%) showed MYC amplification at baseline but they did not show high MYC levels by immunohistochemistry. Because MYC overexpression has been described as a common mechanism of resistance to multiple drugs[19], it is likely that the numerous lines of treatment received by patients entering a phase 1 study contributed to its stabilization and/or amplification.

Women and men were equally represented, and an Eastern Cooperative Oncology Group (ECOG) performance status of 0 and 1 was distributed in a similar manner across patients. Median age was 60.5 years. All patients were treated on a weekly basis by 30–45-min intravenous infusion of either 0.48, 1.44, 2.88, 4.32, 6.48 or 9.72 mg kg^{-1} OMO-103 (n = 1, 1, 3, 5, 9 and 3, respectively). One cycle of treatment was defined as 3 weeks (that is, three infusions).

An overview of general safety is shown in Fig. 1d, and treatment-related adverse events (TRAEs) in Fig. 1e. The most common TRAEs were mainly grade 1 infusion-related reactions (IRRs), including chills, fever, nausea, rash and hypotension (Fig. 1e and Extended Data Table 1). In total, ten of the 22 patients developed IRRs and six experienced them only once while the other four experienced them multiple times. In seven patients the IRR occurred after the first infusion, starting several hours (2–5) after the end of the infusion and lasting only 1 h or, in the worst case, disappearing overnight. Fifty-eight TRAEs (80.5%) were grade 1, 12 (16.6%) were grade 2 and one (1.4%) was grade 3. The only grade 3 IRR observed was in a patient with ovarian carcinoma (OVCA) who had already received 12 lines of treatment and shown a similar reaction to cisplatin, in addition to intolerance to certain antibiotics (including amoxicillin), and therefore this reaction was considered as neither a dose-limiting toxicity (DLT) nor dose dependent, but patient dependent. Higher DLs (5 and 6) were associated with more IRRs, but those were easily prevented with standard (pre)medication. Four patients had a temporary interruption (about 40 min) of the study drug infusion due to IRR (grade 1). In one patient this happened twice while for the others it occurred only once. Another patient developed a grade 2 IRR and so the study drug was interrupted but, as progression of disease was discovered on the same day, treatment was discontinued permanently. One DLT, a grade 2 pancreatitis, was observed at DL5 in a patient with pancreatic ductal adenocarcinoma (PDAC). This case was discussed with the safety monitoring committee (SMC) and, even though the event did not fulfill the criterion of grade 3, it was decided to classify it as DLT to be on the side of safety. This patient was removed from the study, and recovered quickly and completely. This was the only patient—along with the one with IRR grade 3—to be removed from the study due to a TRAE. In total there were 18 serious adverse events but only one of these was considered drug related (the previously mentioned grade 3 IRR). One patient left the study after only one infusion because he developed brain metastases, which were an exclusion criterion for the study. Two patients showed progression of the disease with eventual fatal outcome (grade 5); both had advanced PDAC.

No maximum tolerated dose (MTD) was reached and, overall, the drug was considered safe and tolerable across all DLs. The recommended phase 2 dose (RP2D) was established at DL5, equivalent to 6.48 mg kg^{-1}, based on safety, preliminary antitumor activity, PK, positive target engagement and biomarkers (see below).

PK studies

The PK profile of OMO-103 was studied in serum during dose escalation, and absolute levels of OMO-103 were quantified from tissue biopsies. A summary of the biopsy schedule and samples obtained is shown in Extended Data Table 2. The average PK profile for each DL is shown in Fig. 2a, and descriptive statistics for the parameters are provided in Extended Data Table 3. Nonlinearity was observed above DL5, where the area under the curve (AUC) increased with dose in a nonproportional manner while clearance and volume of distribution diminished after multiple dosing, indicating tissue saturation. Although terminal drug half-life in serum samples was estimated at approximately 40 h, this value is probably an underestimation because PK serum samples were collected only up to 96 h following treatment and OMO-103 showed greater persistence and integrity in tumor tissue compared with that in serum samples. Indeed, using a previously described mass spectrometry (MS) approach based on the detection of four different peptides spanning the entire protein sequence[18], we were able to detect OMO-103 in patient biopsies even 19 days following the last infusion (Fig. 2b,c).

Antidrug antibodies (ADAs) were also analyzed to evaluate the potential immunogenicity of OMO-103. No ADAs were detected at any

https://doi.org/10.1038/s41591-024-02805-1

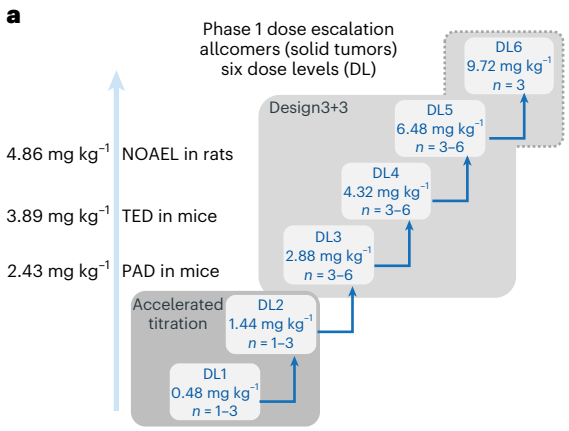

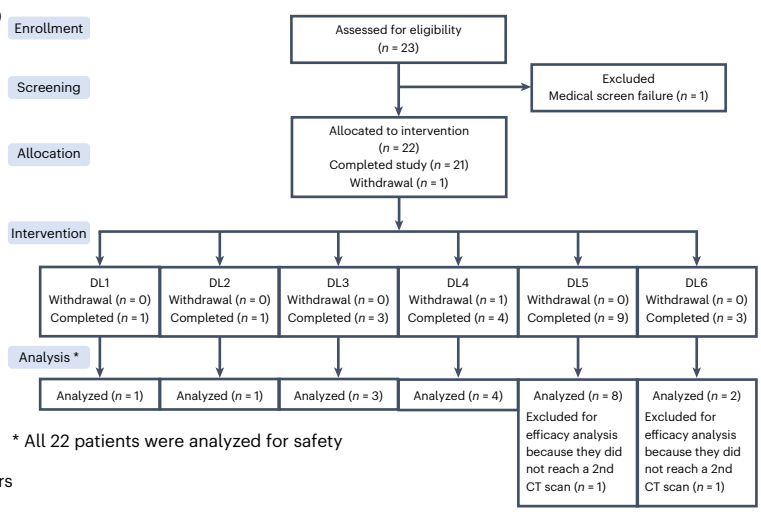

c

Subjects: *n*	OMO-103 dose level						
	0.48 mg kg^{-1} (*n* = 1)	1.44 mg kg^{-1} (*n* = 1)	2.88 mg kg^{-1} (*n* = 3)	4.32 mg kg^{-1} (*n* = 5)	6.48 mg kg^{-1} (*n* = 9)	9.72 mg kg^{-1} (*n* = 3)	Total (*n* = 22)
Female, *n*° (%)	0	1 (100)	1 (33)	3 (60)	4 (44)	2 (66)	11 (50)
Age, median (range), years	32	61	70 (56–73)	61 (44–71)	60 (44–70)	62 (52–65)	60.5 (32–73)
ECOG PS, *n*° (%)							
0	1 (100)	1 (100)	3 (100)	2 (40)	5 (55)	0	12 (55)
1	0	0	0	3 (60)	4 (44)	3 (100)	10 (45)
Cancer type, *n*° (%)							
PDAC	0	1 (100)	1 (33)	1 (20)	4 (44)	1 (33)	8 (36)
CRC	1 (100)	0	0	1 (20)	3 (33)	2 (67)	7 (32)
SARC	0	0	0	1 (20)	0	0	1 (5)
SCLC	0	0	0	1 (20)	0	0	1 (5)
SGC	0	0	1 (33)	0	0	0	1 (5)
Pleuromesothelioma (PLMSTO)	0	0	1 (33)	0	0	0	1 (5)
NSCLC	0	0	0	0	1 (11)	0	1 (5)
TNBC	0	0	0	0	1 (11)	0	1 (5)
OVCA	0	0	0	1 (20)	0	0	1 (5)
Previous lines of therapy, median (range)	5 (5)	3 (3)	3 (3–5)	4 (3–12)	4 (2–6)	4 (3–4)	4 (2–12)

d

Subjects: *n*	OMO-103 dose level						
	0.48 mg kg^{-1} (*n* = 1)	1.44 mg kg^{-1} (*n* = 1)	2.88 mg kg^{-1} (*n* = 3)	4.32 mg kg^{-1} (*n* = 5)	6.48 mg kg^{-1} (*n* = 9)	9.72 mg kg^{-1} (*n* = 3)	Total (*n* = 22)
TEAEs	11	4	16	20	86	17	154
Related TEAEs	4	0	13	5	43	8	73
Grade ≥3 TEAEs	0	0	0	7	8	3	18
Related grade ≥3	0	0	0	1	0	0	1
Serious TEAEs	0	0	0	7	9	2	18
TEAEs leading to death	0	0	0	0	1	1	2
TEAEs leading to treatment discontinuation	0	0	0	2	1	0	3
IRRs	1	0	9	3	28	2	43

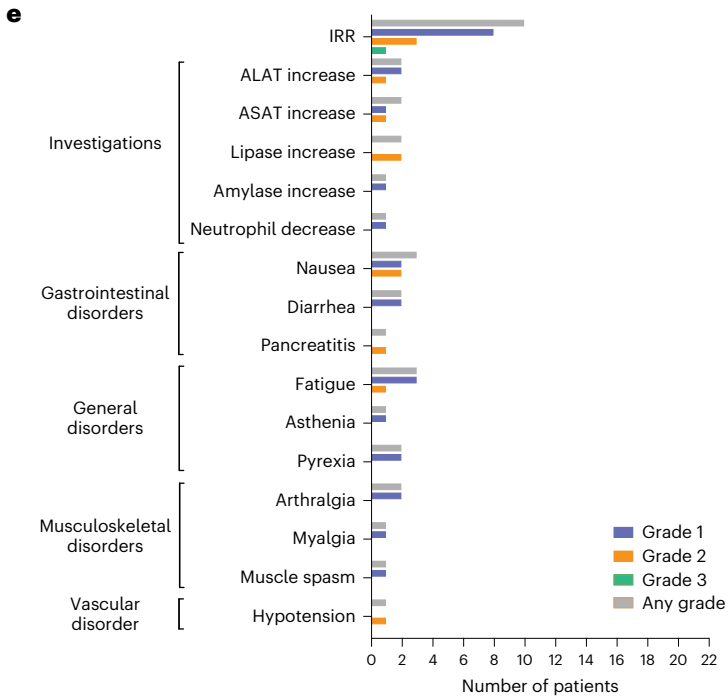

Fig. 1 | Overall trial design and safety. a, Schematic of dose-escalation design. PAD, pharmacologically active dose; TED, therapeutically effective dose; NOAEL, no observed adverse effect level; *n*, number of patients. **b**, CONSORT flow diagram. **c**, Demographic and baseline characteristics. ECOG PS, ECOG performance status. **d**, Overall safety. TEAE, treatment-emergent adverse event. **e**, TRAEs (*n* = 22). System organ class and symptoms are shown. SCLC, small cell lung cancer; NSCLC, non-small cell lung cancer; TNBC, triple-negative breast cancer; ALAT, alanine aminotransferase; ASAT, aspartate aminotransferase.

https://doi.org/10.1038/s41591-024-02805-1

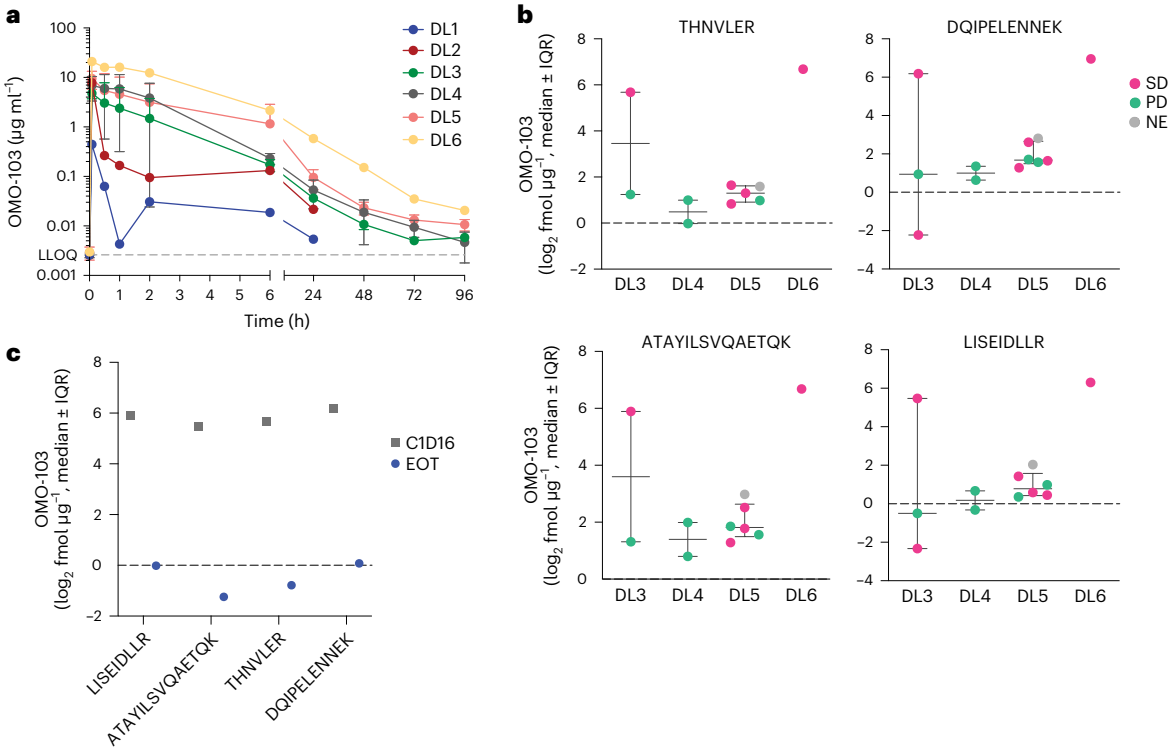

Fig. 2 | PK of OMO-103 in serum and detection in patient biopsies. a, PK profiles at different DLs following a single intravenous infusion of OMO-103 ($n = 22$). LLOQ, lower limit of quantification. Statistical average value and standard deviation are shown. **b**, Quantification of functional Omomyc by MS in FFPE on-treatment biopsies from MYCure patients for DL3–6 following administration of at least three intravenous infusions of OMO-103 ($n = 12$). The sequence of peptides used for detection of the Omomyc protein is indicated on top of the *x* axis. Median value and interquartile range (IQR) are shown. **c**, Results from end-of-treatment (EOT) biopsy of a patient with PDAC from DL3 who remained for >6 months in the study and had received their last infusion 19 days before biopsy, compared with those obtained at cycle 1, day 16 (C1D16). NE, not evaluable.

DL, even following long-term treatment (up to cycle 12 (C12)), except in one patient at DL5 who also showed elevated levels of rheumatoid factor, often considered a confounding element in ADA assessment[20] (Extended Data Table 4).

Antitumor activity

Nineteen patients were evaluable for efficacy. Clinical response to the drug was evaluated by computed tomography (CT) scan following 9 weeks of treatment (three cycles) and every 9 weeks thereafter. In addition, the Guardant360 assay, which detects cell-free circulating tumor DNA in blood specimens and evaluates 73 genes, was used as a complementary surrogate measure of tumor response[21]. Twelve patients reached this time point (patient progress throughout the various phases is summarized in Fig. 1b). Eight patients showed stable disease (SD) at best response, at DL ranging from 2 to 6, with duration of disease stabilization thereafter ranging from 35 to 765 days. These patients included two with PDAC, three with colorectal cancer (CRC), one with NSCLC, one with fusocellular sarcoma (SARC) and one with salivary gland carcinoma (SGC). The other ten patients did not reach the prescheduled 9-week CT scan due to either rapid, early progression of disease or had presented with grade 2 pancreatitis or grade 3 IRR as reported above, and hence were withdrawn from the study. A complete evaluation of all patients is shown in Fig. 3 and Extended Data Table 5. The change in percentage of target lesions compared with baseline throughout the study and at best response is shown in Fig. 3b and 3c, respectively. Among these, some standout cases are described in greater detail below.

One patient with PDAC in DL3 received OMO-103 as a fourth line of treatment and remained in the study for approximately 7 months. This patient achieved 8% tumor shrinkage of target lesions according to response evaluation criteria in solid tumors (RECIST) v.1.1 at the first scheduled CT scan, and 83% reduction in ctDNA following 11 weeks on treatment as measured by the Guardant360 assay (Fig. 3d and Supplementary Table 1). Indeed, the variant allele frequency dynamics of the three somatic alterations identified by Guardant360 showed a slight initial increase in SMAD4 E330K and APC T2481fs (from 0.33 and 0.90% to 0.52 and 1.87%, respectively) after 3 weeks, while APC fell markedly under the limit of detection 8 weeks later and SMAD4 decreased to 0.15% variant allele frequency (Fig. 3d). The HRAS variant remained under the detection limit from week 3 onwards and was never again detected; interestingly, when evaluating the change in total radiographic burden of disease (that is, sum of the volume of all lesions) the patient showed a 49% reduction in volume as best response following OMO-103 treatment (Fig. 3e,f).

One patient with fusocellular sarcoma entered the study at DL4 following five previous lines of treatment. He had not benefited from the previous two lines but remained on treatment with OMO-103 for approximately 8 months.

Finally, the patient affected by a SGC (initially treated at DL3 then escalated to DL4) was maintained on treatment under compassionate use following study completion and was stable for approximately 26 months without any AEs.

It is also worth mentioning that the patient with OVCA who abandoned the study because of a grade 3 IRR underwent a CT scan following two cycles with OMO-103, showing stabilization of the disease and a 30% drop in ctDNA (Supplementary Table 1).

Importantly, no correlation was observed between MYC levels (measured by *H*-score) and clinical response (SD versus progressive disease (PD)) (Extended Data Fig. 1).

https://doi.org/10.1038/s41591-024-02805-1

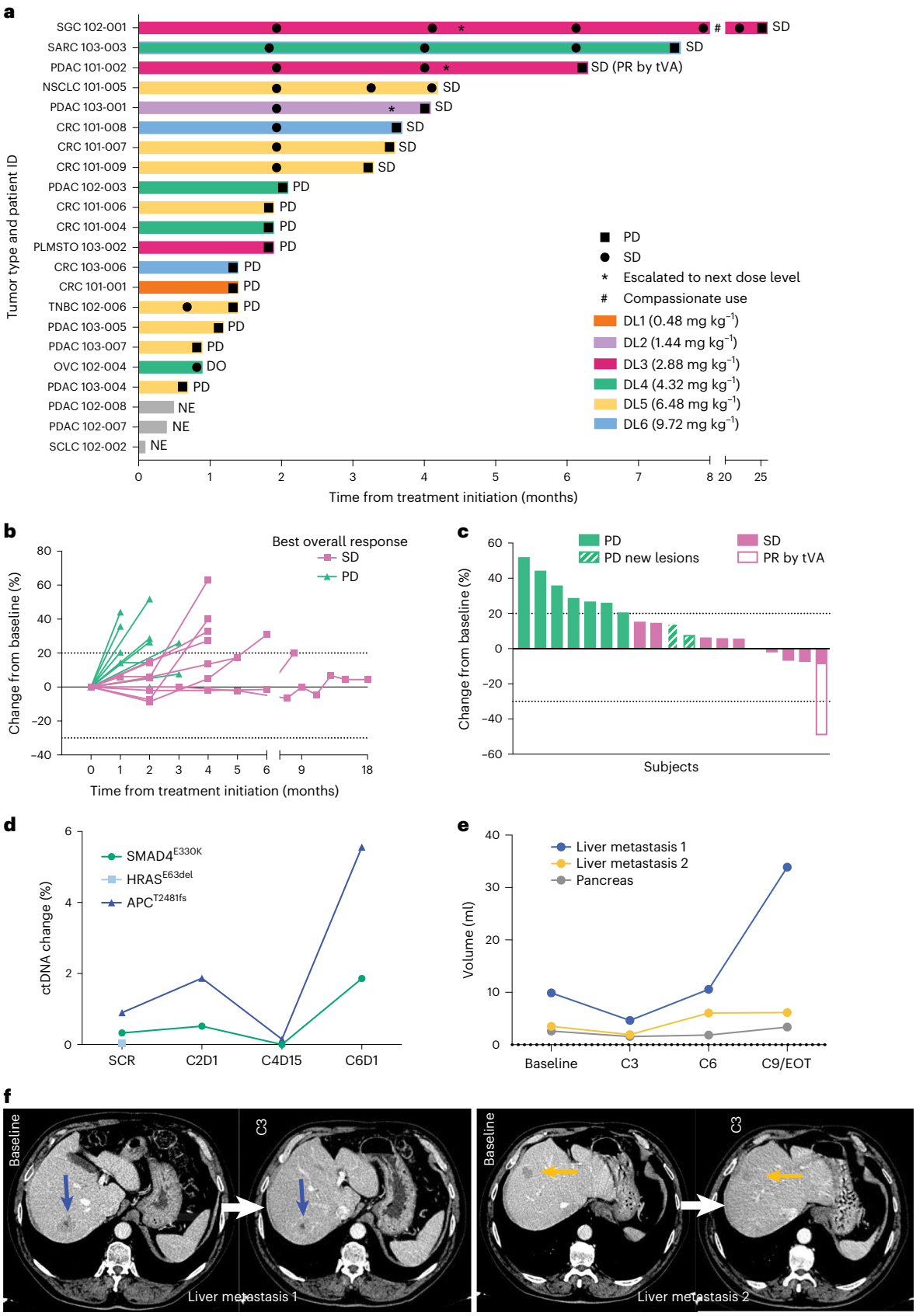

Fig. 3 | Evaluation of tumor response in all cohorts and time-dependent disease evaluation in one patient with PDAC. a, Swimmer plot of 22 enrolled patients. SD, stable disease; PD, progressive disease; DO, dropout; PR, partial response; tVA, Total volumetric analysis. **b**, Spider plot showing changes in target lesion volume from 19 evaluable patients. **c**, Waterfall graph indicating change in volume of target lesions (RECIST v.1.1) at best response of 19 evaluable patients. **d**, ctDNA dynamics of the three somatic alterations identified by Guardant360. **e**,**f**, Baseline, C3, C6 and C9/EOT volume measurement of individual lesions by CT scan (**e**) and representative images (**f**). Blue and yellow arrows indicate lesions quantified in **e**.

https://doi.org/10.1038/s41591-024-02805-1

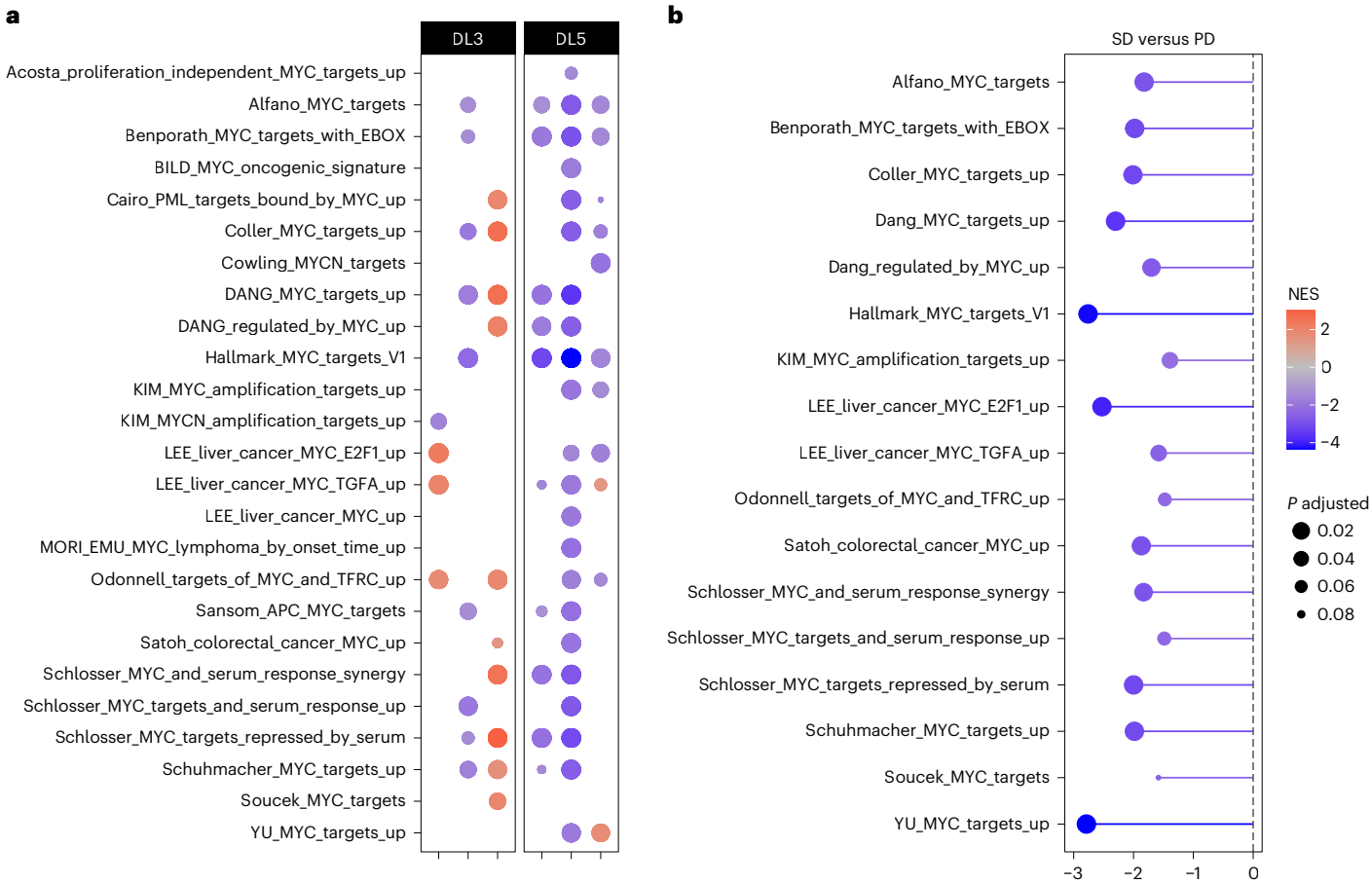

Fig. 4 | Target engagement analysis by DSP. a,**b**, In DL3 and 5, three paired biopsies each were analyzed ($n = 6$ in total). **a**, GSEA comparing the status of each MYC gene set in on-treatment (C1D15)** versus pretreatment biopsies. Normalized enrichment score (NES) is represented by a color scale from red (enriched post treatment) to blue (enriched in pretreatment compared with post), while adjusted *P* value is represented by circle size. For each patient, three to five regions of interest were compiled. **b**, Lollipop graph representing comparison by GSEA of the status of MYC gene sets in samples from patients with SD versus PD. NES is represented by the length of the lollipop and color scale, while the adjusted *P* value is represented by circle size.

OMO-103 treatment is associated with target engagement

Because MYC is a pleiotropic transcription factor, its main function is transcriptional regulation. Previously published work demonstrated that MYC inhibition by Omomyc does not necessarily change MYC levels but consistently impairs its transcriptional activity[6,15,16,22]. Hence, to evaluate target engagement by OMO-103 we performed transcriptomic analysis. To do so, patient biopsies were subjected to digital spatial profiling (DSP), which allowed RNA sequencing of regions of interest and assessment of MYC transcriptional signature by gene set enrichment analysis (GSEA). The study was performed on paired pre- and on-treatment biopsies (Extended Data Table 2). This stringent criterion allowed the analysis of three patients each in DL3 and DL5. DSP results were then cross-compared with published MYC transcriptional fingerprints (Fig. 4a). This analysis revealed a shutdown of multiple MYC transcriptional signatures in one patient in DL3 and in three in DL5, thus correlating the more frequent transcriptional changes with the higher DL. Moreover, patients with SD showed a more profound shutdown compared with those with PD (Fig. 4b).

In addition, we evaluated the transcriptional impact of OMO-103 on immune- and cancer-related programs (Extended Data Fig. 2a). In line with the immunosuppressive role of MYC in the tumor immune microenvironment, several immune-related gene sets were upregulated following its inhibition by OMO-103, especially those related to T cell-mediated immunity. In regard to MYC signature shutdown, immune-activating and tumor-suppressive phenotypes were more profound in patients from DL5 than from DL3 (Extended Data Fig. 2a).

Of note, the analysis of MYC transcriptional signatures was also performed on pan-cytokeratin (PANCK)-negative (nontumor) cells and showed a MYC fingerprint shutdown also in the tumor microenvironment (Extended Data Fig. 2b), demonstrating that the MYC-inhibitory effect of OMO-103 is both tumor cell autonomous and nonautonomous, reflecting the biological role of MYC in both compartments[2].

To complement the transcriptomic analysis, ultradeep protein profiling by MS was applied for analysis of MYC target downregulation at the protein level. Despite the limited sample size (a total of eight paired biopsies from two patients each with SD and PD) that prevented statistical considerations, this analysis showed that 110 out of 179 proteins from the MYC Hallmarks gene set were downregulated in patients with SD compared with 35 out of 179 in those with PD (Extended Data Fig. 2c). Similarly, 37 out of 56 direct MYC targets had reduced protein levels following treatment in patients with SD compared with only three out of 56 in those with PD (Extended Data Fig. 2d), once again correlating clinical benefit with more efficient shutdown of MYC targets.

Predictive and pharmacodynamic liquid biomarkers

As mentioned above, besides having a role in tumor growth, MYC is a well-known modulator of antitumor immune suppression, able to reinstruct the tumor microenvironment towards a tumor-promoting and immune-tolerant phenotype[2,23]. We previously showed that, by inhibition of MYC, Omomyc can reprogram the tumor microenvironment through vascular remodeling and cytokine–chemokine modulation[9,15,23]. Hence, to look for noninvasive biomarkers of response to

OMO-103, blood sampling from patients was performed at baseline and during treatment, with serum analyzed by Luminex technology for circulating soluble factors associated with inflammatory processes and potential cytokine release syndrome. Of note, none of the patients showed any sign of such a potential syndrome following treatment.

We initially searched for potential pretreatment biomarkers capable of predicting response to therapy. At baseline, patients that presented with SD at C3 showed significantly lower levels of soluble macrophage inflammatory protein 1-beta (MIP-1β), interleukin-8 (IL-8), CD62 antigen-like family member E (CD62E, also known as E-selectin) and granulocyte-macrophage colony-stimulating factor (GM-CSF) compared with those shown by patients with PD (Fig. 5a). In addition, binomial logistic regression analysis showed that CD62E, IL-8, MIP-1β and GM-CSF had odds ratios (ORs) clearly <1 (CD62E, 0.125 (CI 0.016–1.004, $P = 0.053$, $R^2 = 0.46$); IL-8, 0.088 (CI 0.007–1.037, $P = 0.050$, $R^2 = 0.609$); and MIP-1β, 0.002 (CI 0–13.822, $P = 0.17$, $R^2 = 0.826$)), showing a negative association with SD at C3 (Fig. 5b). It is important to note that, while trends toward significance were observed for CD62E and IL-8, limited sample size and interpatient variability may have contributed to the lack of statistical significance. Of note, in this context MIP-1β showed the strongest association with SD but did not display a statistically significant OR due to the high variability of chemokine levels in the PD group and reduced number of evaluable patients. The trends observed in these data suggest potential associations, warranting further investigation in larger cohorts to validate these preliminary findings.

To investigate the predictive power of these identified soluble factors for clinical response to OMO-103, we fitted the values of each factor to a univariate logistic regression model. The performance of these models was evaluated with receiver operating characteristic (ROC) curve analysis. ROC–AUC values were 0.97 for MIP-1β, 0.89 for IL-8, 0.87 for CD62E and 0.85 for GM-CSF, all >0.8, indicating that these models represent excellent SD outcome predictors (Extended Data Fig. 3a).

Most interestingly, subjecting the Luminex data to QLattice technology enabled us to identify a distinct signature predictive of disease stabilization in response to OMO-103 and independent of oncological indication or previous treatment. Such a signature encompasses four of the soluble factors identified as significantly lower at baseline for patients with SD. These factors generate three independent models of prediction (Fig. 5c) that include the combination of two soluble markers. Again, ROC curve analysis suggested that these three combination models are outstanding predictors of SD outcome and that their predictive power is improved compared with that of their individual models (CD62E + MIP-1β, AUC = 0.96; MCP-1 + MIP-1β, AUC = 0.98; CD62E + IL-8, AUC = 0.98; Extended Data Fig. 3b).

Subsequently, following the same process and rationale, we sought to determine a pharmacodynamic signature of response during treatment. In this case we found three soluble factors transiently induced following infusion with OMO-103 starting from C3 onwards (Fig. 6a). This signature had already been detected ~2–3 weeks before the predefined 9-week CT scan assessment and was observed only in patients who then showed SD while it was absent in those with PD. Indeed, all patients showing SD following 9 weeks of treatment displayed significantly increased levels of interferon-γ (IFNγ), CD62E and interleukin-17A (IL-17A) at several time points following OMO-103 infusion. In contrast, in patients with PD the levels of these markers remained completely stable (Fig. 6a). Of note, the transient increase in levels of these soluble factors was observed at the onset of C3 in all patients showing SD, except in patient no. 102-001, who nevertheless proceeded to evidence increase at C6. This signature was independent of oncological indication or previous treatments (Supplementary Table 2).

As described above, further analysis of these data with the QLattice technology generated one independent model for each of the soluble factors capable of efficiently distinguishing patients with SD and PD (Fig. 6b). Once again, ROC curve analysis showed that the AUC for these three models was very close to 1 (IFNγ, AUC = 0.96; CD62E, AUC = 0.96; and IL-17A, AUC = 1; Extended Data Fig. 4).

Notably, the transient increase in serum levels of IFNγ, CD62E and IL-17A following treatment is associated with maintenance of SD; once patients start to progress, their peak levels decrease or even disappear (Extended Data Fig. 5). This was seen in patient nos. 101-002 and 103-003 at C9, the time point at which they transited from SD to PD according to RECIST. Note that none of the patients showed ADAs at any point during treatment, suggesting that this cytokine signature is a specific antitumor immune response (Extended Data Table 4).

Discussion

The most deregulated oncogene in human cancers is MYC but it has remained an elusive target in cancer biology for decades. Here we present what, to our knowledge, is the first successful phase 1 clinical trial validating the safety and tolerability of a first-in-modality direct MYC inhibitor, OMO-103, derived from the most extensively characterized MYC inhibitor to date[6,15,17]. OMO-103 showed safety, causing mainly grade 1 side effects in patients—mostly infusion-related reactions of low grade that are often demonstrated by biologics. The drug also showed suitable PK properties up to the recommended dose, with low or absent immunogenicity.

In addition, the study indicated encouraging signs of drug activity based on both clinical response and assessment of molecular target engagement and biomarkers of response. With regard to clinical activity it is important to highlight that, even though there was no objective response to treatment according to RECIST criteria, at least one patient demonstrated 49% tumor reduction by total tumor burden volume quantification and half of the patients (all showing very resistant and advanced disease) benefited from OMO-103, undergoing disease stabilization. Notably, one patient received treatment under compassionate use after the study was closed and benefited from it for approximately 26 months.

Importantly, drug activity was also supported by target engagement as demonstrated by the shutdown of bona fide MYC-driven transcriptional signatures in patient biopsies. Although this analysis was performed on a limited number of samples it should be noted that, to our knowledge, this is the first time that such an effect has ever been shown in patients with any experimental anti-MYC therapeutic[5,17].

Taking advantage of the double role of MYC in both intra- and extracellular programs of tumorigenesis, we were also able to identify soluble biomarkers of response to MYC inhibition in serum samples. Our findings suggest both a predictive and pharmacodynamic signature. These can be detected by liquid biopsies, and include well-known soluble factors involved in activation of the immune response. Following treatment with OMO-103, patients showing disease stabilization presented transiently increased levels of IFNγ, CD62E and IL-17A. IFNγ is a pleiotropic cytokine with well-known antitumor activity, mainly promoting antigen presentation and activating cytotoxic immune cells. In addition, it also has direct cancer cell-specific antitumor effects such as inhibition of proliferation and induction of apoptosis[24,25]. Based on these properties, IFNγ treatment is considered potentially useful as an adjuvant immunotherapy[26]. In contrast, the exact role of IL-17 in tumor immunity is still under debate, mainly due to the wide variety and high plasticity of IL-17-producing cells. However, the secretion of IL-17 along with other effector cytokines such as IFNγ can exert potent antitumor effects boosting tumor-specific T cell responses through enhanced dendritic and cytotoxic T cell recruitment to the tumor bed[27]. Finally, CD62E is expressed on cytokine-activated endothelial cells and mediates leukocyte migration into inflamed tissues, a fundamental prerequisite for the entry of antitumor effector cells to the tumor site[28]. These results are in line with those obtained from differential gene expression analysis of tumor biopsies, where several gene sets related

https://doi.org/10.1038/s41591-024-02805-1

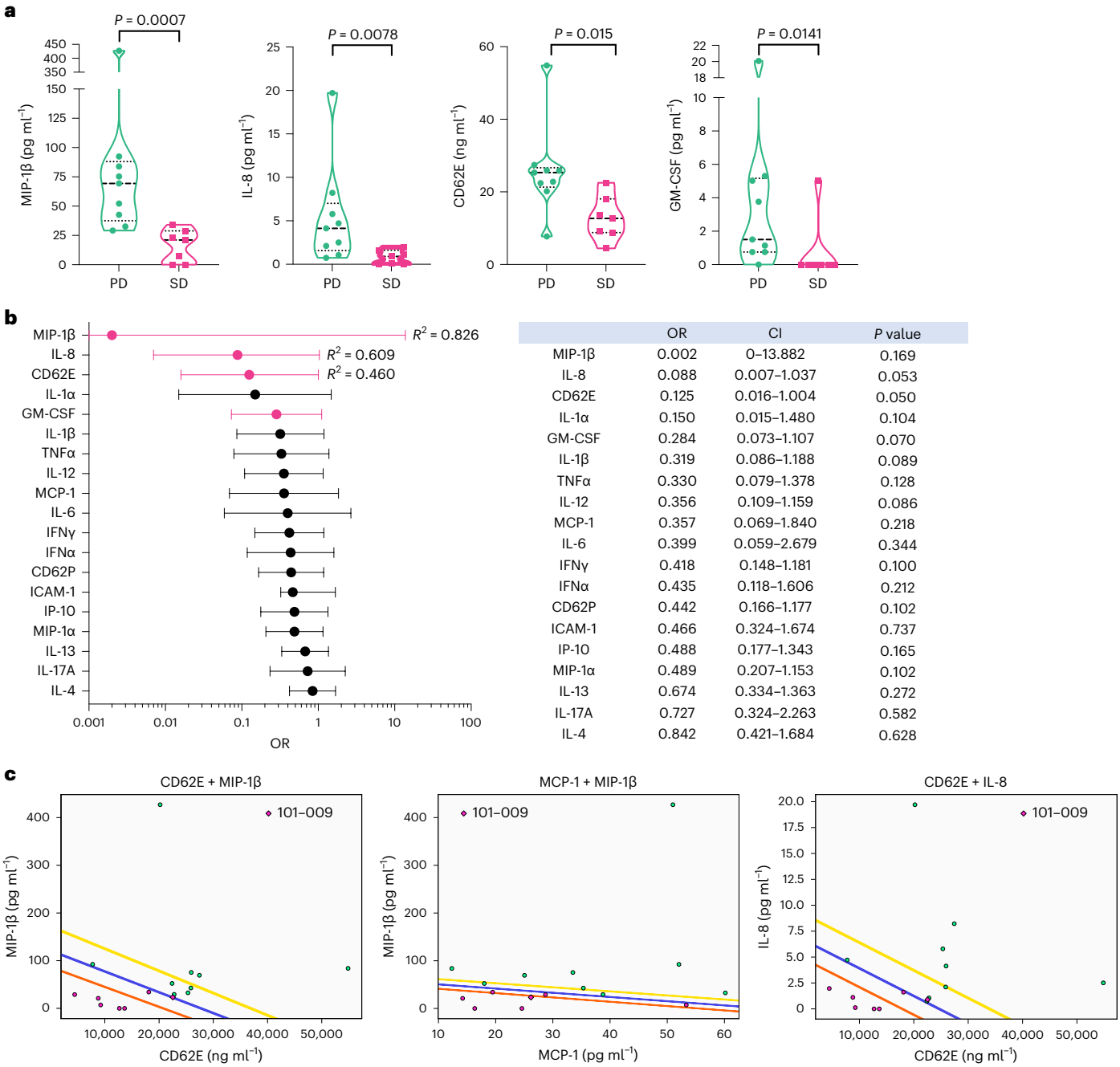

	OR	CI	*P* value
MIP-1β	0.002	0–13.882	0.169
IL-8	0.088	0.007–1.037	0.053
CD62E	0.125	0.016–1.004	0.050
IL-1α	0.150	0.015–1.480	0.104
GM-CSF	0.284	0.073–1.107	0.070
IL-1β	0.319	0.086–1.188	0.089
TNFα	0.330	0.079–1.378	0.128
IL-12	0.356	0.109–1.159	0.086
MCP-1	0.357	0.069–1.840	0.218
IL-6	0.399	0.059–2.679	0.344
IFNγ	0.418	0.148–1.181	0.100
IFNα	0.435	0.118–1.606	0.212
CD62P	0.442	0.166–1.177	0.102
ICAM-1	0.466	0.324–1.674	0.737
IP-10	0.488	0.177–1.343	0.165
MIP-1α	0.489	0.207–1.153	0.102
IL-13	0.674	0.334–1.363	0.272
IL-17A	0.727	0.324–2.263	0.582
IL-4	0.842	0.421–1.684	0.628

Fig. 5 | Patients that clinically benefited from OMO-103 showed low baseline levels of MIP-1β, IL-8, CD62E and GM-CSF, with model pairings of different soluble factors providing outstanding outcome predictors. a–**c**, Levels of soluble factors were measured in patient serum samples at pretreatment using the Luminex technique. **a**,**b**, Nine patients with PD and seven with SD were included in the analyses. **a**, Patients showing disease stabilization at cycle 3 displayed significantly lower levels of MIP-1β, IL-8, CD62E and GM-CSF compared with those with PD (median shown). A two-sided Mann–Whitney *U*-test, with no adjustment for multiple comparisons, was used for statistical analysis. **b**, Binomial logistic regression analysis of the association of cytokine and chemokine levels at pretreatment with the probability of disease stabilization. ORs of soluble factors in patients are shown in the forest plot (left) and summary table (right); mean and CI are shown. **c**, Soluble factor combination models generated using QLattice technology; data from nine patients with PD and six with SD were used to generate the models. Plots of combination models CD62E + MIP-1β, MCP-1 + MIP-1β and CD62E + IL-8 are shown in relationship to patient response. SD and PD are indicated by pink and green dots, respectively. Colored lines correspond to confidence bands: blue indicates the mean, orange 95% CI and yellow 5% CI. Patient no. 101-009 is marked with a rhombus because their data were not available at the time of generation of the models and were later included.

to T cell immunity and migration were upregulated following OMO-103 treatment. Notably, all three soluble factors have been associated with wound healing and wound resolution, an interplay often defective in cancer and metastasis[29–32], strictly related to MYC biology[33]. The transient increase of these proinflammatory soluble factors that occurs only in patients with SD is distinct from a chronic inflammatory response and may indicate an antitumor immune response triggered by OMO-103 treatment. Importantly, none of the patients showing the pharmacodynamic signature presented ADAs.

In conclusion, we believe that these findings and the safety profile of OMO-103 encourage further investigation of its clinical activity and safety in specific indications. In addition, a combination of MYC inhibition with other treatments—chemotherapy, personalized medicine and immunotherapy—could increase their efficacy both in contexts

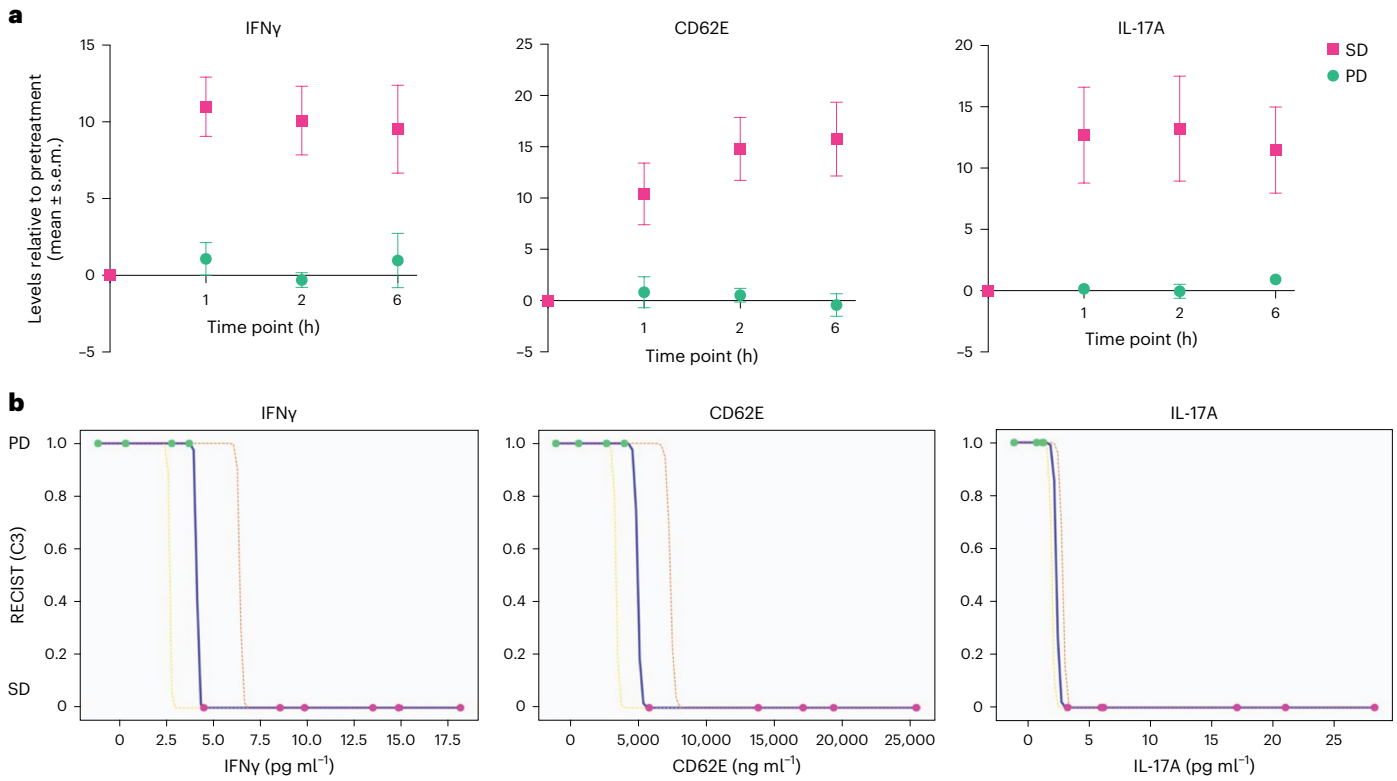

Fig. 6 | Following OMO-103 infusion, patients with disease stabilization at C3 showed significantly increased levels of IFNγ, CD62E and IL-17A, which can be used to identify patients with SD or PD. a,**b**, Levels of different soluble factors were measured in patient serum samples taken at different time points following OMO-103 treatment and were determined using the Luminex technique. Four and six patients with PD and SD, respectively, were included in the analysis. **a**, At the onset of C3, patients with disease stabilization at the following CT scan showed a significant increase in levels of IFNγ ($P = 0.000148$), CD62E ($P = 0.000338$) and IL-17A ($P = 0.0013$) following OMO-103 infusion compared with patients with PD. Mean and s.e.m. are shown. A two-sided Welch's *t*-test was used with Bonferroni correction to adjust for multiple comparisons. **b**, Individual IFNγ, CD62E and IL-17A models generated with QLattice technology. Maximum serum levels of the indicated cytokines were used to generate the models. Serum levels of patients with PD and SD are indicated as 1 and 0, respectively. Colored lines correspond to confidence bands: blue indicates the mean, yellow 5% CI and orange 95% CI.

where MYC is not overexpressed as well as where it is amplified or overexpressed (a common mechanism of drug resistance[19]).

Among the limitations of this clinical study, it did not include MYC amplification or overexpression as inclusion criteria, based on the concept that MYC addiction is not necessarily dependent on its absolute levels but more on its tonic, deregulated signaling[34]. In addition, we saw no correlation between Omomyc efficacy and MYC levels in preclinical studies[6,14,16]. Nevertheless, the question remains as to whether varying MYC expression levels might reveal a different sensitivity to OMO-103, especially in earlier lines of treatment. Future clinical studies will hopefully shed light on this matter.

The identification of pharmacodynamic and predictive biomarkers is based on a limited and heterogenous number of patients, with very different previous lines of treatment (as is inherent in any phase I study in oncology), and hence their validity and potential antitumorigenic role require further testing in a larger and more homogenous patient population. The identified signatures are indeed currently being tested in a new clinical study with OMO-103 in combination with standard-of-care (SoC) chemotherapy (ClinicalTrials.gov identifier: NCT06059001), where the predictive signature is being used for patient selection.

Online content

Any methods, additional references, Nature Portfolio reporting summaries, source data, extended data, supplementary information, acknowledgements, peer review information; details of author contributions and competing interests; and statements of data and code availability are available at https://doi.org/10.1038/s41591-024-02805-1.

References

1. Dang, C. V., Reddy, E. P., Shokat, K. M. & Soucek, L. Drugging the 'undruggable' cancer targets. *Nat. Rev. Cancer* **17**, 502–508 (2017).
2. Dhanasekaran, R. et al. The MYC oncogene – the grand orchestrator of cancer growth and immune evasion. *Nat. Rev. Clin. Oncol.* **19**, 23–36 (2022).
3. Stine, Z. E., Walton, Z. E., Altman, B. J., Hsieh, A. L. & Dang, C. V. MYC, metabolism, and cancer. *Cancer Discov.* **5**, 1024–1039 (2015).
4. Nie, Z. et al. Dissecting transcriptional amplification by MYC. *eLife* **9**, e52483 (2020).
5. Whitfield, J. R., Beaulieu, M. E. & Soucek, L. Strategies to inhibit Myc and their clinical applicability. *Front. Cell Dev. Biol.* **5**, 10 (2017).
6. Masso-Valles, D. & Soucek, L. Blocking Myc to treat cancer: reflecting on two decades of Omomyc. *Cells* **9**, 883 (2020).
7. Soucek, L. et al. Design and properties of a Myc derivative that efficiently homodimerizes. *Oncogene* **17**, 2463–2472 (1998).
8. Annibali, D. et al. Myc inhibition is effective against glioma and reveals a role for Myc in proficient mitosis. *Nat. Commun.* **5**, 4632 (2014).
9. Sodir, N. M. et al. Endogenous Myc maintains the tumor microenvironment. *Genes Dev.* **25**, 907–916 (2011).
10. Soucek, L. et al. Modelling Myc inhibition as a cancer therapy. *Nature* **455**, 679–683 (2008).
11. Soucek, L. et al. Omomyc, a potential Myc dominant negative, enhances Myc-induced apoptosis. *Cancer Res.* **62**, 3507–3510 (2002).

12. Fiorentino, F. P. et al. Growth suppression by MYC inhibition in small cell lung cancer cells with TP53 and RB1 inactivation. *Oncotarget* **7**, 31014–31028 (2016).
13. Soucek, L. et al. Inhibition of Myc family proteins eradicates KRas-driven lung cancer in mice. *Genes Dev.* **27**, 504–513 (2013).
14. Zacarias-Fluck, M. F. et al. Reducing MYC's transcriptional footprint unveils a good prognostic gene signature in melanoma. *Genes Dev.* **37**, 303–320 (2023).
15. Beaulieu, M. E. et al. Intrinsic cell-penetrating activity propels Omomyc from proof of concept to viable anti-MYC therapy. *Sci. Transl. Med.* **11**, eaar5012 (2019).
16. Massó-Vallés, D. et al. MYC inhibition halts metastatic breast cancer progression by blocking growth, invasion, and seeding. *Cancer Res. Commun.* **2**, 110–130 (2022).
17. Whitfield, J. R. & Soucek, L. The long journey to bring a Myc inhibitor to the clinic. *J. Cell Biol.* **220**, e202103090 (2021).
18. Beaulieu, M.-E. et al. Pharmacokinetic analysis of Omomyc shows lasting structural integrity and long terminal half-life in tumor tissue. *Cancers* **15**, 826 (2023).
19. Donati, G. & Amati, B. MYC and therapy resistance in cancer: risks and opportunities. *Mol. Oncol.* **16**, 3828–3854 (2022).
20. Tatarewicz, S., Miller, J. M., Swanson, S. J. & Moxness, M. S. Rheumatoid factor interference in immunogenicity assays for human monoclonal antibody therapeutics. *J. Immunol. Methods* **357**, 10–16 (2010).
21. Lanman, R. B. et al. Analytical and clinical validation of a digital sequencing panel for quantitative, highly accurate evaluation of cell-free circulating tumor DNA. *PLoS ONE* **10**, e0140712 (2015).
22. Jung, L. A. et al. OmoMYC blunts promoter invasion by oncogenic MYC to inhibit gene expression characteristic of MYC-dependent tumors. *Oncogene* **36**, 1911–1924 (2017).
23. Whitfield, J. R. & Soucek, L. Tumor microenvironment: becoming sick of Myc. *Cell. Mol. Life Sci.* **69**, 931–934 (2012).
24. Martinez-Sabadell, A., Arenas, E. J. & Arribas, J. IFNgamma signaling in natural and therapy-induced antitumor responses. *Clin. Cancer Res.* **28**, 1243–1249 (2022).
25. Zaidi, M. R. The interferon-gamma paradox in cancer. *J. Interferon Cytokine Res.* **39**, 30–38 (2019).
26. Korentzelos, D., Wells, A. & Clark, A. M. Interferon-gamma increases sensitivity to chemotherapy and provides immunotherapy targets in models of metastatic castration-resistant prostate cancer. *Sci. Rep.* **12**, 6657 (2022).
27. Kuen, D. S., Kim, B. S. & Chung, Y. IL-17-producing cells in tumor immunity: friends or foes? *Immune Netw.* **20**, e6 (2020).
28. Nourshargh, S. & Alon, R. Leukocyte migration into inflamed tissues. *Immunity* **41**, 694–707 (2014).
29. Bernard, N. J. IL-17A heals wounds. *Nat. Immunol.* **23**, 1134 (2022).
30. Ishida, Y., Kondo, T., Takayasu, T., Iwakura, Y. & Mukaida, N. The essential involvement of cross-talk between IFN-gamma and TGF-beta in the skin wound-healing process. *J. Immunol.* **172**, 1848–1855 (2004).
31. Sundaram, G. M., Quah, S. & Sampath, P. Cancer: the dark side of wound healing. *FEBS J.* **285**, 4516–4534 (2018).
32. Worthen, C. A. et al. CD26 identifies a subpopulation of fibroblasts that produce the majority of collagen during wound healing in human skin. *J. Invest. Dermatol.* **140**, 2515–2524 (2020).
33. Stojadinovic, O. et al. Molecular pathogenesis of chronic wounds: the role of beta-catenin and c-Myc in the inhibition of epithelialization and wound healing. *Am. J. Pathol.* **167**, 59–69 (2005).
34. Murphy, D. J. et al. Distinct thresholds govern Myc's biological output in vivo. *Cancer Cell* **14**, 447–457 (2008).

Publisher's note Springer Nature remains neutral with regard to jurisdictional claims in published maps and institutional affiliations.

Open Access This article is licensed under a Creative Commons Attribution 4.0 International License, which permits use, sharing, adaptation, distribution and reproduction in any medium or format, as long as you give appropriate credit to the original author(s) and the source, provide a link to the Creative Commons license, and indicate if changes were made. The images or other third party material in this article are included in the article's Creative Commons license, unless indicated otherwise in a credit line to the material. If material is not included in the article's Creative Commons license and your intended use is not permitted by statutory regulation or exceeds the permitted use, you will need to obtain permission directly from the copyright holder. To view a copy of this license, visit http://creativecommons.org/licenses/by/4.0/.

© The Author(s) 2024

[1]Vall d'Hebron Institute of Oncology, Barcelona, Spain. [2]Peptomyc S.L., Barcelona, Spain. [3]START Madrid-FJD-Hospital Fundación Jiménez Díaz, Madrid, Spain. [4]START Madrid-CIOCC-Centro Integral Oncológico Clara Campal, Madrid, Spain. [5]Institució Catalana de Recerca i Estudis Avançats, Barcelona, Spain. [6]Department of Biochemistry and Molecular Biology, Universitat Autònoma de Barcelona, Bellaterra, Spain. [7]These authors contributed equally: Elena Garralda, Marie-Eve Beaulieu. ✉e-mail: Lsoucek@vhio.net

Methods

Study design and patient population

MYCure (NCT04808362) is a first-in-human, open-label, multicenter, phase 1 dose-escalation study of six DLs evaluating the safety of OMO-103 across solid tumors conducted at three sites in Spain.

Complete and signed written informed consent was obtained from patients for inclusion in the study. There was no remuneration for participation in the trial but there was compensation for travel expenses.

The study included histologically or cytologically proven advanced solid tumors for which there was no curative therapy, that had progressed on SoC treatment, were intolerant to it or had no available SoC or for which SoC was unacceptable. Patients had to demonstrate measurable disease according to RECIST v.1.1 criteria[35] as demonstrated by CT/magnetic resonance imaging and documented progression on or following the last line of therapy. They also had to present an ECOG performance status of up to 1, life expectancy of ≥12 weeks and adequate organ function.

For patient demographics please refer to Fig. 1c. Women and men were equally represented in the study. Sex of participants was determined based on self-reporting.

OMO-103 was administered by weekly intravenous infusion over 30–45 min, one treatment cycle corresponding to three infusions. Patients were treated until progression. Safety follow-up was 1 month.

The starting dose of 0.48 mg kg^{-1} was determined based on nonclinical toxicology and efficacy studies (anticipated pharmacologically active dose) and subsequent conversion to human equivalent dose. This dose was anticipated to result in safety margins of tenfold compared with the predicted minimum efficacious dose.

An accelerated titration design was used. Following the first two DLs with one patient each, the 3 + 3 design was applied. The first patient at each DL was monitored for the first week of C1; if considered safe, the other patients in the cohort were treated simultaneously. The initial plan was to test five DLs and enroll six patients in DL5. Because no DLTs (excepting one grade 2 pancreatitis) were seen, it was agreed with the SMC to add a further DL—that is, DL6. However, starting at DL5 an increased number of IRRs were observed and tissue saturation was detected (PK curve), and this was also confirmed at DL6. It was therefore decided to concentrate on DL5, which was then backfilled and chosen as the RP2D.

Note that the original study design also included an amendment (no. 3) to enroll double-hit lymphoma (DHL) patients; however, this amendment was considered only at a much later time compared with the start of the trial because enrollment of DHL patients was planned for phase 2. Because the phase 2 part of the study was canceled, no DHL patients were eventually enrolled in phase 1.

Tumor biopsy (from either the primary tumor or metastases) had to be obtained from patients during both screening and treatment, following at least 2 weeks of treatment and three infusions (at around C1D15).

The study was conducted according to the principles of Good Clinical Practice and the Declaration of Helsinki, and approvals from the Country Competent Authority and Central Ethics Committee were obtained before starting any study-related procedures. The study was registered according to country-specific regulations.

Safety monitoring committee members were responsible for safeguarding the interests of patients, assessing the safety of the study drug during the study and any study-specific interventions required. The committee reviewed toxicity and other relevant data at the completion of each DL cohort and issued a recommendation pertaining to dose escalation. Intrapatient dose escalation was allowed when a higher dose was considered safe by the SMC.

Outcomes

The primary objective of the study was to determine the safety and tolerability of single-agent OMO-103. Secondary objectives were RP2D, PK, PD and preliminary antitumor activity, including identification of potential biomarkers.

Dose-limiting toxicity, MTD and RP2D: Toxicities were graded according to the Common Terminology Criteria for Adverse Events (NCI–CTCAE) v.5.0. A DLT was defined as a grade 3 or higher adverse event according to NCI–CTCAE, considered at least possibly related to the study drug and occurring during the 21-day observation period. MTD was defined as the DL below that associated with DLTs in either two out of three or two out of six patients. MTD was not reached in this study.

RP2D was selected based on clinical safety/tolerability, antitumor activity, PK and PD data.

Clinical response was assessed using CT according to RECIST (v.11) criteria at pretreatment and every 9 weeks thereafter.

ctDNA assay

Blood samples for exploratory biomarker ctDNA analyses were obtained and subjected to the next-generation sequencing panel Guardant360 at Guardant Health, Inc. The Guardant360 assay detects single-nucleotide variants, indels, fusions and copy number alterations in 73 genes[36]. All plasma specimens collected at (1) baseline (except for one patient that was removed from the study due to brain metastases), were genotyped ($n = 21$) when available at C2D1 ($n = 18$) and selected at C4 and/or C6 ($n = 7$) and at (2) progression ($n = 3$) (Supplementary Table 1).

Volumetric tumor assessment

All contrast-enhanced CT scans were acquired within 28 days before the treatment starting day, at 9 weeks of treatment (that is, after three cycles) and then every 9 weeks while on treatment. We further explored responses by changes in volume in those patients achieving SD/partial response/complete response as best response according to RECIST v.1.1. All tumors (primary and metastatic disease) of at least 1 cm in diameter (that is, considered measurable according to RECIST v.1.1) per patient were segmented using the semiautomatic segmentation tool of 3DSlicer (v.4.11.0)[37] by an experienced radiologist in oncologic imaging (R.P.-L.). Pixel size and number were recorded to calculate total tumor volume (pixel size × number) per patient and compute changes in volume from baseline.

PK and ADAs

Serum samples for PK assessment were taken at C1, 3, 6 and 9, just before dosing, and at 5 min, 30 min, 1 h, 2 h, 6 h, 24 h, 48 h, 72 h and 96 h following the end of infusion (the time points of 48, 72 and 96 h were applied only to patients from DL3 onwards). Serum was isolated using standard procedures and cryopreserved at −80 °C until use. Concentrations of OMO-103 were determined using a validated electrochemiluminescence assay (ECLA) method. PK parameters (t1/2, AUClast, AUCinf, AUCinf/D, Vz and Cl) were estimated using noncompartmental analysis following single and multiple administrations.

Serum samples for ADA assessment were taken at screening, before dosing at C1, 2 and 3 and then every three cycles, and at the end of both treatment and follow-up. Serum was isolated using standard procedures and cryopreserved at −80 °C until use. The presence of anti-Omomyc ADAs was measured using a validated ECLA method performed according to the bioanalytical guidelines of the European Medicines Agency and Food and Drug Administration. The analytical method consisted of an ECL assay in a bridging format. Serum samples were incubated in the presence of biotin-Omomyc and sulfoTAG-Omomyc and the resulting immune complexes (biotin-Omomyc/anti-Omomyc antibodies/sulfoTAG-Omomyc) were captured using a streptavidin plate and measured by ECLA.

Both PK and ADA assays were conducted in compliance with the Principles of Good Laboratory Practices regulations.

DSP GeoMx Human Whole Transcriptome Atlas

Paired formalin-fixed, paraffin-embedded (FFPE) biopsies collected before and during treatment (Extended Data Table 2) were sectioned and stained for PANCK to identify tumor cells. Samples were prepared according to tumor type following Nanostring's procedure then loaded into the DSP instrument for selection of between one and five polygonal regions of interest (500–600 µm per sample).

Digital spatial profiling data were analyzed using the GeoMxTools R package (v.3.0.1). Quality check and preprocessing of the data were performed using the standard parameters as suggested by Nanostring (https://github.com/Nanostring-Biostats/GeomxTools). Quartile 3 normalization was used to normalize data. For differential gene expression analysis within patient samples (pre- and on-treatment biopsies) we used linear mixed-effect models with the functions provided by GeoMxTools, while comparisons between groups of patients (SD and PD) were performed using the limma R package (v.3.52.4). GSEA was conducted using the clusterProfiler R package (v.4.4.4). MYC gene sets were obtained from the chemical and genetic perturbations collection, Biological Process ontology gene sets were obtained from the Gene Ontology collection and hallmark gene sets were obtained from the Hallmark collection, all in the molecular signatures database. Data were plotted using the ggplot2 R package (v.3.3.6).

Pharmacodynamics

Blood samples were taken at pretreatment (just before patients received the first OMO-103 infusion and before every subsequent infusion) and at 1, 2 and 6 h following infusion. Serum was then isolated using standard procedures and cryopreserved at −80 °C until use. Levels of cytokines, chemokines and other soluble factors were measured by the Luminex technique using the Inflammation 20-Plex Human ProcartaPlex kit (Invitrogen) that includes GM-CSF, IFNα, IFNγ, IL-1α, IL-1β, IL-4, IL-6, IL-8, IL-10, IL-12p70, IL-13, IL-17A, TNFα, IP-10, MCP-1, MIP-1α, MIP-1β, ICAM-1, CD62E (E-selectin) and CD62P (P-selectin). Plates were read using the MAGPIX detection system. Soluble factor levels were extrapolated from standard curves using ProcartaPlex Analysis Software v.2.2.0. For analysis of the predictive and pharmacodynamic signature, only patients evaluable for response were considered.

MYC immunohistochemical analysis

For evaluation of MYC expression, pretreatment ($n = 18$) and on-treatment ($n = 13$) biopsies from 19 patients were analyzed using 100 µl of a ready-to-use solution of anti-c-MYC (Y69) rabbit monoclonal primary antibody (Roche) per sample, following the protocol described in ref. 38. Briefly, staining was performed using a Benchmark ULTRA autostainer (Ventana Medical Systems) and detection was carried out with the UltraView Universal DAB Detection kit (no. 760–500, Ventana Medical Systems). For assessment of MYC a semiquantitative approach was used in which *H*-scores were generated by multiplying staining intensity (0, no staining; 1, weak; 2, moderate; 3, strong) by the percentage (0–100) of positive cells.

OMO-103 quantification by LC–MS parallel reaction monitoring and ultradeep data-independent acquisition profiling in patient biopsies

Samples were prepared according to the Biognosys Suite of Proteomics for FFPE samples, including sonication, deparaffinization and homogenization, using the Covaris LE220Rsc sonication device. Samples were then processed individually on a KingFisher Flex overnight at 37 °C according to the Biognosys Suite of Proteomics, which includes reduction, alkylation and digestion of peptides using trypsin (Promega, ratio of 1:50 protease to total protein) and Lys-C (Fujifilm Wako Chemicals, ratio of 1:200 protease to total protein).

Clean-up for MS was carried out using an Oasis HLB µElution plate (30 µm, Waters) according to the manufacturer's instructions. Peptides were dried to complete dryness using a SpeedVac system and dissolved in LC solvent A (1% acetonitrile in water and 0.1% formic acid (FA)) containing Biognosys indexed retention time peptide mix for retention time calibration. Peptide concentrations in MS-ready samples were measured using the mBCA assay (Thermo Scientific Pierce).

For OMO-103 quantification, five stable isotope-labeled reference peptides were spiked into the final peptide samples at known concentrations (Vivitide; the quality grade of the reference peptides was ±10% quantification precision and >95% purity).

For LC–MS parallel reaction monitoring (LC–PRM) measurement, 1 µg of peptides per sample was injected into an in-house-packed C18 column (PicoFrit emitter with 75 µm inner diameter, 60 cm length and 10 µm tip from New Objective, packed with 1.7 µm of Charged Surface Hybrid C18 particles from Waters) on a Thermo Scientific Easy nLC 1200 nanoLC system connected to a Thermo Scientific Q Exactive mass spectrometer equipped with a standard nanoelectrospray source. LC solvents were: A, 1% acetonitrile in water with 0.1% FA and B, 20% water in acetonitrile with 0.1% FA. The LC gradient was 0–59% solvent B over 54 min followed by 59–90% B for 12 s and 90% B for 8 min (total gradient length 67 min). A scheduled run in PRM mode was performed before data acquisition for retention time calibration using the Biognosys indexed retention time concept[39]. The data acquisition window per peptide was 7 min. Signal processing and data analysis were carried out using SpectroDive 11.0—Biognosys' software for multiplexed PRM data analysis based on mProphet[39,40]. A *Q*-value filter of 1% was applied.

For ultradeep data-independent acquisition (DIA) LC–tandem MS measurements, 2 µg of peptides or all peptides (Biognosys ID 3, 4 and 7) was loaded on an in-house-packed reversed-phase column of a Thermo Scientific NeoVanquish UHPLC nanoLC system connected to a Thermo Scientific Orbitrap Exploris 480 mass spectrometer equipped with a Nanospray Flex ion source and a FAIMS Pro ion mobility device (Thermo Scientific). LC solvents were: A, water with 0.1% FA and B, 80% acetonitrile and 0.1% FA in water. The nonlinear LC gradient was 1–50% solvent B for 172 min followed by a column-washing step in 90% B for 5 min, and a final equilibration step of 1% B for one column volume with flow rate set to a ramp of 500–250 nl min^{-1} (min 0, 500 nl min^{-1}; min 172, 250 nl min^{-1}, washing at 500 nl min^{-1}). The FAIMS DIA method consisted of an applied compensation voltage of one full-range MS1 scan and 34 DIA segments, as previously adopted[41,42].

The DIA MS data were analyzed using directDIA+ in Spectronaut software (Biognosys, v.18.4) with the false discovery rate for peptide and protein levels set to 1%. A human UniProt.fasta database (*Homo sapiens*, 2023-07-01) was used for the search engine, allowing for two missed cleavages and variable modifications (N-term acetylation, methionine oxidation and methylation) and cysteine carbamidomethylation as fixed modification. The assay library (protein inventory) generated in this project was used for analysis. The hyper reaction monitoring measurements analyzed with Spectronaut were normalized using local regression normalization[43].

Statistical methods and analysis

Sample size was determined based on clinical rather than statistical considerations. Twenty-two patients were recruited, this being consistent with phase 1 dose-finding studies.

Statistical analyses were performed by the Clinical Research Organization Simbec-Orion using SAS v.9.4 or later (SAS Institute).

Safety and tolerability were analyzed through the incidence of AEs, serious AEs and specific laboratory abnormalities (worst grade) in each DL. Toxicities were tabulated by type and grade for all doses and presented using frequencies based on CTCAE v.5.0. All subjects who received at least one dose of the study drug were evaluable for safety (safety analysis set).

Antitumor activity was assessed using RECIST v.1.1 and included ORR, progression-free survival and disease control rate. All efficacy endpoints were summarized and analyzed descriptively using the full analysis set (all patients in the SAF who completed at least one follow-up

assessment, defined as any primary assessment variable recording using RECIST v.1.1).

PK analyses were performed from experimental data and using actual sampling times and dosing levels of each subject via the PKSolver add-in program for Microsoft Excel, by means of a noncompartmental approach.

Predictive signatures of soluble factors

To determine whether the levels of the examined soluble factors were different between patients with PD and SD at pretreatment, a univariate analysis was performed. A two-sided Mann–Whitney U-test with no adjustment for multiple comparisons was used to determine whether the levels of soluble factors between the two groups were significantly different. To calculate OR the levels of soluble factors were transformed using the $\log_2$ scale. Individual (univariate) binary logistic regression models, in which the exponential of the coefficients can be directly interpreted as OR, were applied using the statistical software package SPSS statistics (SPSS). Logistic regression was used to measure the strength of the association between levels of soluble factors at baseline and response to OMO-103 treatment. The diagnostic accuracy of the individual soluble factors in identifying patients with SD was estimated using ROC–AUC, which was also used as a global measure to compare the predictive power of each individual soluble factor. A cutoff of AUC = 0.8 was used for selection of soluble factors with good predictive power. The analysis was performed by Abzu fitting of a logistic regression model to each soluble factor individually, with RECIST v.1.1 evaluation at C3 as the binary output variable. The Python package Scikit-learn was used to fit the models[44].

Combinations of soluble factors that can correctly stratify patients between PD and SD were found using QLattice modeling technology (Abzu)[45]. QLattice was run within a leave-one-out cross-validation loop, excluding a single patient at each iteration. ROC–AUC was also calculated for the combination models to determine its prediction accuracy and power. Confidence interval bands of the models were estimated using the parameter values of all models found.

Pharmacodynamic/response signatures of soluble factors

To determine whether the increase in the serum levels of various soluble factors was different between SD and PD patients at the onset of C3, their levels relative to pretreatment of this particular cycle were calculated. A total of ten patients were considered in this analysis (six SD and four PD); one patient showing the signature at C6 rather than at C3 was excluded from the analysis. *P* value was used to reject the null hypothesis. A two-sided Welch's *t*-test was used to determine whether the levels of cytokines, chemokines and other soluble factors between the two groups were significantly different. Bonferroni correction was used to adjust for multiple comparisons. Again, QLattice modeling technology (Abzu) was used to determine single models that could estimate the soluble factor levels that distinguish between patients with SD and PD. To generate the models, for each patient the levels of only one time point (the maximum level of each soluble factor) were considered. QLattice was run within a leave-one-out cross-validation loop, excluding a single patient at each iteration. ROC–AUC was also calculated for the single models to determine their prediction accuracy and power (as described above). Confidence interval bands of the models were estimated using the parameter values of all models found.

The datasets generated during and/or analyzed during the current study, as well as the custom codes used for its analyses, are available from the corresponding author on reasonable request.

Reporting summary

Further information on research design is available in the Nature Portfolio Reporting Summary linked to this article.

Data availability

The raw data for DSP analysis are available at https://doi.org/10.5281/zenodo.10420686. On reasonable request, and subject to review, Peptomyc will provide the multiplex data that support the findings of this study. Subject to certain criteria, conditions and exceptions, Peptomyc may also provide access to the related individual deidentified participant data. The protocol and statistical analysis plan for MYCure have been uploaded to ClinicalTrials.gov. Source data are provided with this paper.

References

35. Eisenhauer, E. A. et al. New response evaluation criteria in solid tumours: revised RECIST guideline (version 1.1). *Eur. J. Cancer* **45**, 228–247 (2009).
36. Odegaard, J. I. et al. Validation of a plasma-based comprehensive cancer genotyping assay utilizing orthogonal tissue- and plasma-based methodologies. *Clin. Cancer Res.* **24**, 3539–3549 (2018).
37. Hayes, S. A. et al. Comparison of CT volumetric measurement with RECIST response in patients with lung cancer. *Eur. J. Radiol.* **85**, 524–533 (2016).
38. Serna, G. et al. Targeted multiplex proteomics for molecular prescreening and biomarker discovery in metastatic colorectal cancer. *Sci. Rep.* **9**, 13568 (2019).
39. Escher, C. et al. Using iRT, a normalized retention time for more targeted measurement of peptides. *Proteomics* **12**, 1111–1121 (2012).
40. Reiter, L. et al. mProphet: automated data processing and statistical validation for large-scale SRM experiments. *Nat. Methods* **8**, 430–435 (2011).
41. Tognetti, M. et al. Biomarker candidates for tumors identified from deep-profiled lpasma stem predominantly from the low abundant area. *J. Proteome Res.* **21**, 1718–1735 (2022).
42. Bruderer, R. et al. Optimization of experimental parameters in data-independent mass spectrometry significantly increases depth and reproducibility of results. *Mol. Cell. Proteomics* **16**, 2296–2309 (2017).
43. Callister, S. J. et al. Normalization approaches for removing systematic biases associated with mass spectrometry and label-free proteomics. *J. Proteome Res.* **5**, 277–286 (2006).
44. Abraham, A. et al. Machine learning for neuroimaging with scikit-learn. *Front. Neuroinform.* **8**, 14 (2014).
45. Christensen, N. J. et al. Identifying interactions in omics data for clinical biomarker discovery using symbolic regression. *Bioinformatics* **38**, 3749–3758 (2022).

Acknowledgements

The authors from Vall d'Hebron Institute of Oncology (VHIO) thank the Cellex Foundation for providing research facilities and equipment, and the CERCA Program from the Generalitat de Catalunya for their support on this research. They also acknowledge the State Agency for Research (Agencia Estatal de Investigación) for financial support as Center of Excellence Severo Ochoa (no. CEX2020-001024-S/AEI/10.13039/501100011033). We thank the teams at Abzu and Biognosys for their valuable service and feedback, and M.-A. Morcillo for his help in the interpretation of PK data. This research has received funding from the Generalitat de Catalunya (AGAUR grant no. 2021/SGR 01509); from the European Union Horizon 2020 research and innovation program under grant agreement nos. 872212 and 101144681; from the Ministerio de Ciencia e Innovación, grant no. RTC2019-007067; from the Ministerio de Ciencia, Innovación y Universidades, grant nos. CPP2022-009808 and PLEC2021-007959 by MCIN/AEI/10.13039/501100011033 and European Union NextGenerationEU/PRTR.

Author contributions

E.G. was Principal Investigator of the clinical study, contributed to study design and supervised its execution. M.-E.B. contributed to the study plan, supervised the biomarkers program and contributed to writing of the paper. V.M. coordinated the study at START Madrid-FJD-Hospital Fundación Jiménez Díaz. S.C.-S. planned, coordinated and executed immune-related studies and contributed to writing of the paper. S.M.-M. coordinated and executed the transcriptomic and proteomic studies and contributed to writing of the paper. L.F. and D.M.-V. contributed to PK studies. S.L.-E. contributed to execution of the immune-related studies for biomarker analysis. T.J. contributed to regulatory study material preparation. G.A., E.C.d.l.F., B.D., T.H. and J.M. contributed to clinical study execution. R.P.-L. performed tumor volumetric analysis. O.A. performed bioinformatic analysis of transcriptomic data. V.C.C. contributed to quality and regulatory material preparation. J.R.W. contributed to data analysis and writing of the paper. M.N. led the study plan, protocol design and writing and supervised its execution, and contributed to writing of the paper. L.S. participated in study planning and design, supervised and coordinated the whole study and led writing of the paper. E.C. coordinated the study at the START Madrid-Centro Integral Oncológico Clara Campal and participated in paper revision.

Competing interests

E.G. is Consultant-Advisor for Roche/Genentech, F.Hoffmann/La Roche, Ellipses Pharma, Neomed Therapeutics1, Inc., Boehringer Ingelheim, Janssen Global Services, SeaGen, TFS, Alkermes, Thermo Fisher, Bristol-Myers Squibb, MabDiscovery, Anaveon, F-Star Therapeutics and Hengrui. L.S. is Consultant and CEO of Peptomyc. V.M. is Consultant of Roche, Bayer, BMS, Janssen and Basilea. E.C. is Consultant-Advisor for Nanobiotix, Janssen-Cilag, Roche-Genentech, TargImmune Therapeutics, Servier, Bristol-Myers Squibb, Amunix, Adcendo, Anaveon, AstraZeneca/Medimmune, Chugai Pharma, MonTa, MSD Oncology, Nouscom, OncoDNA, T-Knife, Elevation Oncology, PharmaMar, Ellipses Pharma, Syneos Health, Genmab and Diaccurate. Employment. M.-E.B., S.C.-S., S.M.-M., L.F., S.L.-E., V.C.C., J.M., M.N. and L.S. are employees of Peptomyc. E.C. is an employee of START. Personal financial interests: L.S. and M.-E.B. are cofounders and shareholders of Peptomyc and inventors of patent application no. WO2014180889 A8 that covers the use of the Omomyc miniprotein in medicine, held by VHIO and licenced to Peptomyc. S.C.-S., S.L.-E., L.F., J.R.W. and M.N. are also shareholders of Peptomyc. E.G. performs research for Novartis, Roche, Thermo Fisher, AstraZeneca, Taiho and BeiGene; she is in Speakers Bureau for Merck Sharp & Dohme, Roche, Thermo Fisher, Lilly and Novartis; she runs clinical trials as PI or Co-PI with Agios Pharmaceuticals, Amgen, Bayer, Beigene USA, Blueprint Medicines, BMS, Cellestia Biotech, Debiopharm, F.Hoffmann/La Roche, Ltd, Forma Therapeutics, Genentech, Inc., Genmab B.V., GSK, Glycotope Gmbh, Incyte Biosciences, Incyte Corporation, ICO, Kura Oncology, Inc, Lilly, S.A, Loxo Oncology, Inc, Macrogenics, Inc, Menarini Ricerche Spa, Merck, Sharp & Dohme de España, S.A, Nanobiotix, S.A, Novartis Farmacéutica, S.A, Pfizer, SLU, Pharma Mar, S.A.U, Pierre Fabre Medicament, Principia Biopharma, Inc., Psioxus Therapeutics, Ltd, Sanofi, Sierra Oncology, Inc, Sotio A.S and Symphogen A/S. V.M. is Principal Investigator and receives institutional funding from AbbVie, AceaBio, Adaptimmune, ADC Therapeutics, Aduro, Agenus, Amcure, Amgen, Astellas, AstraZeneca Bayer Beigene BioInvent International AB, BMS, Boehringer, Boheringer, Boston, Celgene, Daichii Sankyo, DEBIOPHARM, Eisai, e-Terapeutics, Exelisis, Forma Therapeutics, Genmab, GSK, Harpoon, Hutchison, Immutep, Incyte, Inovio, Iovance, Janssen, Kyowa Kirin, Lilly, Loxo, MedSir, Menarini, Merck, Merus, Millennium, MSD, Nanobiotix, Nektar, Novartis, Odonate Therapeutics, Pfizer, Pharma Mar, PharmaMar, Principia, PsiOxus, Puma, Regeneron, Rigontec, Roche, Sanofi, Sierra Oncology, Synthon, Taiho, Takeda, Tesaro, Transgene, Turning Point Therapeutics and Upshersmith. E.C. is Principal Investigator and receives institutional funding from START, Pharma Mar, EORTC, Sanofi, BeiGene, Novartis and Merus N.V.; he is a shareholder of START and Oncoart Associated and receives honoraria from HM Hospitales Group; he receives research funding from START; he is President and Founder of Foundation Investigational Therapeutics in Oncological Sciences; and he has a not-for-profit relationship with PharmaMar and the CRIS Cancer Foundation. The other authors declare no competing interests.

Additional information

Extended data is available for this paper at https://doi.org/10.1038/s41591-024-02805-1.

Supplementary information The online version contains supplementary material available at https://doi.org/10.1038/s41591-024-02805-1.

Correspondence and requests for materials should be addressed to Laura Soucek.

Peer review information *Nature Medicine* thanks Cathy Eng, Dean Felsher, Ruitao Lin and the other, anonymous, reviewer(s) for their contribution to the peer review of this work. Primary Handling Editor: Ulrike Harjes, in collaboration with the *Nature Medicine* team.

Reprints and permissions information is available at www.nature.com/reprints.

https://doi.org/10.1038/s41591-024-02805-1

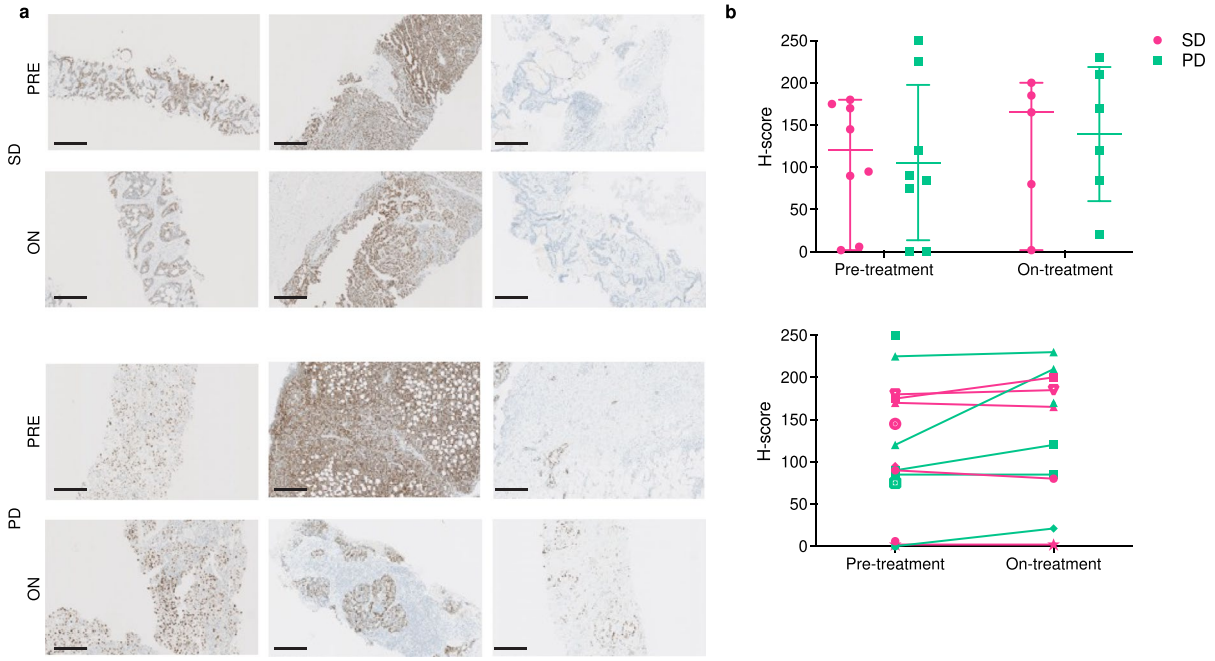

Extended Data Fig. 1 | MYC levels in patient biopsies. (a) Representative images of pre- and on-treatment biopsies from stable and progressive disease patients. **(b)** Quantification of MYC protein levels determined by immunohistochemistry and given as H-score, a semi-quantitative assessment that takes into account the intensity (graded as 0, 1+, 2+, or 3+ for each cell) and percentage of positive cells according to the formula: H-score = [1 × (% cells 1+) + 2 × (% cells 2+) + 3 × (% cells 3+)]. n = 16 patients at pre-treatment. n = 11 patients at on-treatment. In the upper plot, the median value and 95% confidence intervals are shown. In the lower plot, the variation in H-score between pre- and on-treatment is shown per patient, when possible. A mixed-effects analysis with Bonferroni's correction for multiple tests was used.

https://doi.org/10.1038/s41591-024-02805-1

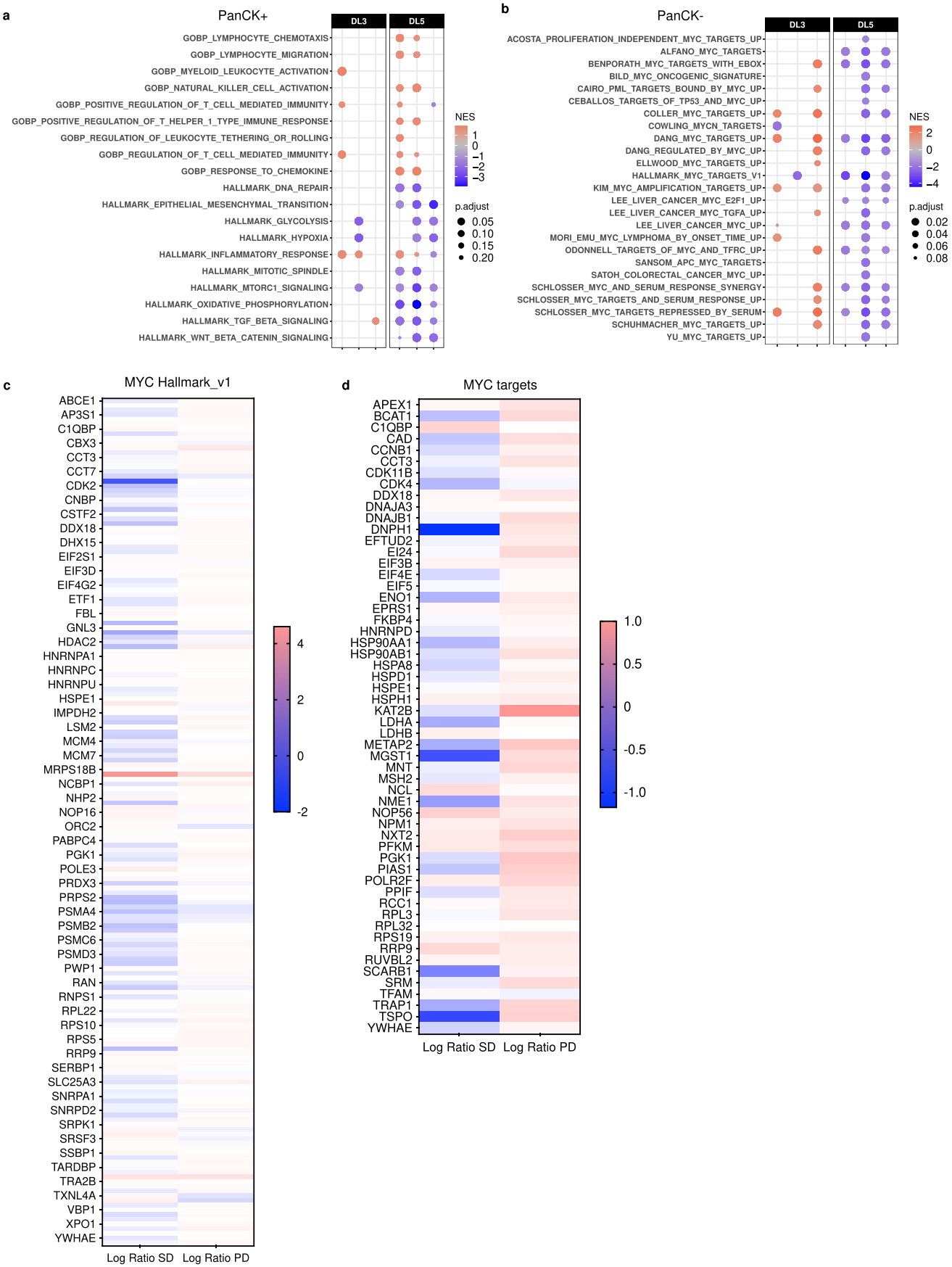

Extended Data Fig. 2 | See next page for caption.

https://doi.org/10.1038/s41591-024-02805-1

Extended Data Fig. 2 | DSP assessment of modulation of additional pathways in the tumor related to cancer and the immune system and target engagement in PanCK- cells, and proteomic analysis of MYC targets. 3 paired biopsies were analyzed in DL3 and 3 in DL5 (n=6 in total). GSEA comparing in on-treatment versus pre-treatment biopsies the **(a)** status of immune- and cancer-related gene sets in the PanCK+ segment and **(b)** status of each MYC gene set in the PanCK- segment. The NES is represented by a color scale from red (enriched post-treatment) to blue (enriched in the pre-treatment compared to the post), while the adjusted p-value is represented by the size of each circle. For each patient, 3–5 regions of interest were compiled. **(c** and **d)** 2 paired biopsies were analyzed in DL3 and 2 in DL5 (n=4 in total) by UltraDeep Protein Profiling. The Log Ratio of SD and PD patients was calculated per protein by dividing on-treatment by pre-treatment values from a subset of **(c)** 179 proteins from the MYC Hallmarks v1 and **(d)** 56 direct targets of MYC. Such values are represented by a color scale from red (upregulated) to blue (downregulated).

https://doi.org/10.1038/s41591-024-02805-1

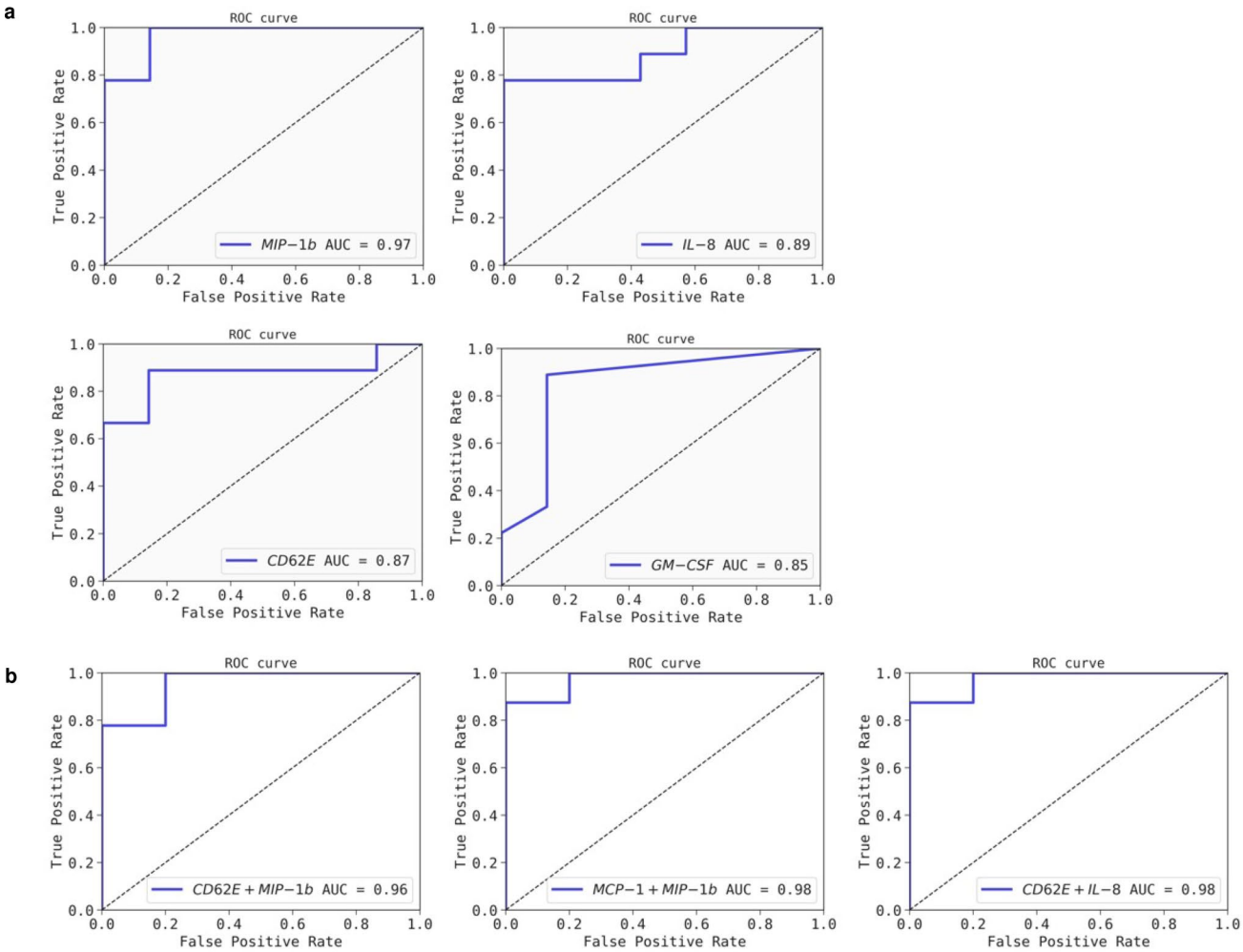

Extended Data Fig. 3 | Receiver Operating Characteristic (ROC) curve analysis of the identified soluble factors and predictive combination models. **(a)** Receiver Operating Characteristic (ROC) curve analysis for individual soluble factors to predict response to OMO-103. Individual ROC curve graphs and their corresponding Area Under the Curve (AUC) scores for each individual soluble factor are shown. Each ROC curve illustrates the relationship between the true positive rate and the false positive rate across various classification thresholds. **(b)** ROC curve analysis and ROC-AUC scores of the predictive combination models are shown below. ROC-AUC scores of the combination models are higher than those of the individual factors, suggesting an increased predictive power.

https://doi.org/10.1038/s41591-024-02805-1

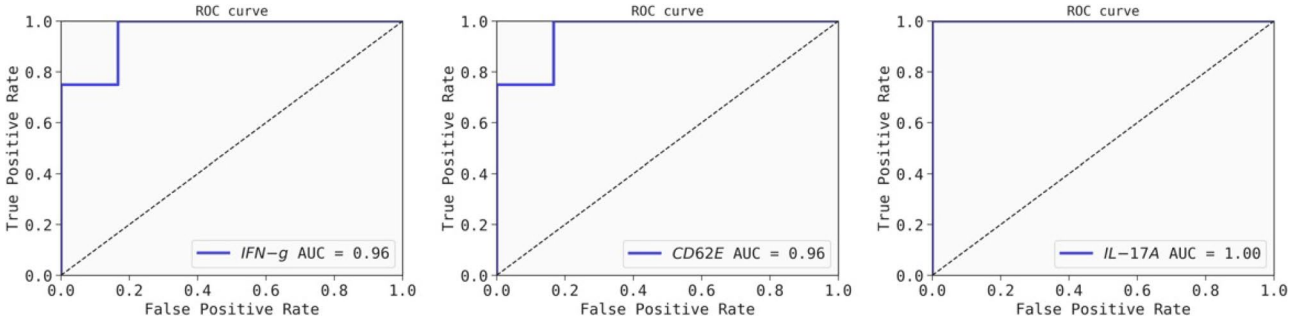

Extended Data Fig. 4 | Receiver Operating Characteristic (ROC) curve analysis of the individual pharmacodynamic models. Receiver Operating Characteristic (ROC) curve analysis of the individual pharmacodynamic models to identify SD vs PD patients upon OMO-103 treatment. Individual ROC curve graphs and ROC-AUC scores for each individual model are shown. Each ROC curve illustrates the relationship between the true positive rate and the false positive rate across various classification thresholds.

https://doi.org/10.1038/s41591-024-02805-1

101-002						
	C3	Model classification	Probability to become PD	C9	Model classification	Probability to become PD
IFN-γ	8.54	SD	0 [90% CI (0; 0)]	3.79	PD	0.998 [90% CI (0;1)]
CD62E	19403.47	SD	0 [90% CI (0; 0)]	3995.9	PD	1 [90% CI (0.001; 1)]
IL-17A	6.16	SD	0 [90% CI (0; 0)]	4.1	SD	0 [90% CI (0; 0)]

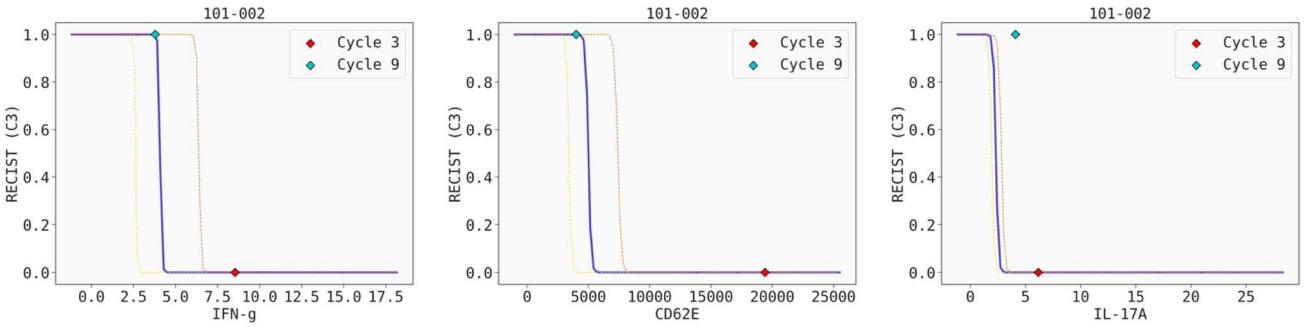

103-003						
	C3	Model classification	Probability to become PD	C9	Model classification	Probability to become PD
IFN-γ	4.46	SD	0 [90% CI (0;1)]	0.127	PD	1 [90% CI (1;1)]
CD62E	5849.89	SD	0 [90% CI (0;1)]	304.8	PD	1 [90% CI (1;1)]
IL-17A	3.23	SD	0 [90% CI (0;0.033)]	1.42	PD	1 [90% CI (0.996;1)]

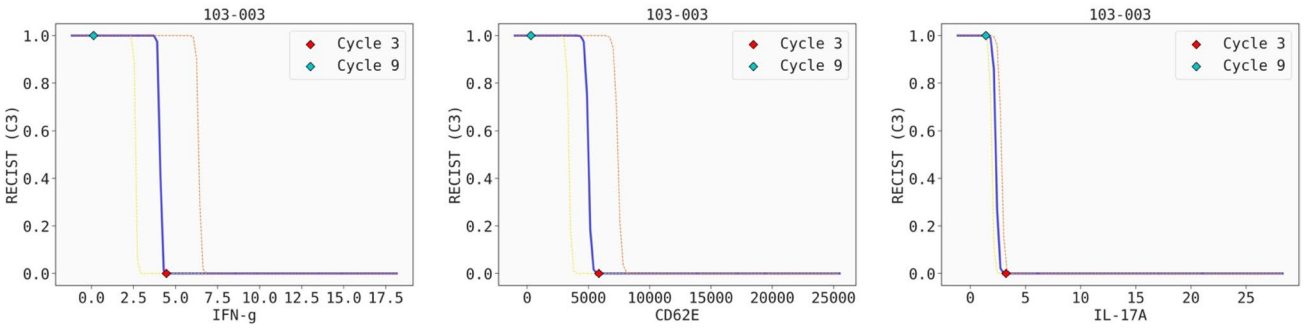

Extended Data Fig. 5 | The pharmacodynamic signature can be associated to maintained SD and is lost upon disease progression. The levels of IFN-γ, CD62E and IL-17A are not transiently increased after OMO-103 infusion for patients 101-002 and 103-003 at C9, time point at which they displayed PD as per RECIST criteria. Tables indicate the values relative to pre-dose at the maximum peak, how the model classifies them in terms of SD or PD, and the probability to become PD according to their maximum relative levels. Graphs of the three independent models show the relative values of each soluble factor at C3 and C9. C3 is marked as a red dot and C9 as a yellow dot. CI: confidence interval.

https://doi.org/10.1038/s41591-024-02805-1

Extended Data Table 1 | Treatment-related adverse events (TRAEs) with severity grade according to the Common Terminology Criteria for Adverse Events version 5.0

SOC and symptom	Grade 1	Grade 2	Grade 3
Injury, poisoning and procedural complications			
IRR	39	3	1
Investigations	5	4	
ALAT increase	2	1	
ASAT increase	1	1	
Lipase increase		2	
Amylase increase	1		
Neutrophil decrease	1		
Gastrointestinal Disorders	4	3	
Nausea	2	2	
Diarrhea	2		
Pancreatitis		1	
General Disorders	8	1	
Fatigue	3	1	
Asthenia	3		
Pyrexia	2		
Musculoskeletal Disorders	4		
Arthralgia	2		
Myalgia	1		
Muscle Spasm	1		
Vascular Disorder		1	
Hypotension		1	

Reported System Organ Class (SOC) and symptoms are shown with the numbers of events. IRR: Infusion Related Reaction; ALAT: Alanine-Aminotransferase; ASAT: Aspartate-Aminotransferase.

https://doi.org/10.1038/s41591-024-02805-1

Extended Data Table 2 | Timepoints for biopsy collection and availability

Patient number	Tumor type	Organ biopsy	Timepoint	Time since last infusion	Dose level	Availability for analysis Y/N
101-002	PDAC	Liver	SCR	-	-	Y
101-002	PDAC	Liver	C1D16	24h	DL3	Y
101-002	PDAC	Liver	EOT	19D	EDL4	Y
102-001	SGC	Lung	SCR	-	-	Y
102-001	SGC	Lung	C1D19	96h	DL3	Y
103-002	PLMSTO	Pleura	PRE-SCR	-	-	Y
103-002	PLMSTO	Lung	C3D16	24h	DL3	Y
103-003	SARC	Soft tissue	PRE-SCR	-	-	Y
102-003	PDAC	Lymph node	SCR	-	-	Y
102-003	PDAC	Lymph node	C1D16	24h	DL4	Y*
101-004	CRC	Lung	SCR	-	-	N**
101-004	CRC	Lung	C1D16	24h	DL4	Y
102-004	OVCA	Liver	SCR	-	-	Y
103-004	PDAC	Liver	PRE-SCR	-	-	Y
103-005	PDAC	Pleura	SCR	-	-	Y
103-005	PDAC	Skin	C1D17	48h	DL5	Y
101-006	CRC	Lung	SCR	-	-	Y
101-006	CRC	Lung	C1D17	48h	DL5	Y
102-006	TNBC	Lymph node	SCR	-	-	N***
102-006	TNBC	Lymph node	C2D16	24h	DL5	Y
101-005	NSCLC	Lung	SCR	-	-	Y
101-005	NSCLC	Lung	C1D16	24h	DL5	Y
101-007	CRC	Lymph node	SCR	-	-	Y
102-008	PDAC	Liver	SCR	-	-	Y
102-008	PDAC	Liver	C1D16	24h	DL5	Y****
103-007	PDAC	Liver	SCR	-	-	Y
101-009	CRC	Liver	SCR	-	-	Y
101-009	CRC	Liver	C1D16	24h	DL5	Y****
103-006	CRC	Soft tissue	SCR	-	-	Y
102-007	PDAC	Liver	SCR	-	-	Y
101-008	CRC	Liver	SCR	-	-	Y
101-008	CRC	Liver	C1D16	24h	DL6	Y****

SCR: screening; PRE-SCR: pre-screening (up to 6 months before entering the study); CXDX: cycle x day x; DL: dose level. Colored in yellow are the patients from whom we only received the pre-treatment biopsy. Y/N: yes or no. * biopsy was lost during DSP processing. ** biopsy did not have tumor tissue. *** biopsy material used up with IHC assessment. **** not evaluated by DSP.

https://doi.org/10.1038/s41591-024-02805-1

Extended Data Table 3 | Summarized descriptive statistics of the pharmacokinetic parameters of OMO-103 after multiple intravenous infusions of OMO-103 with different dose levels

		DL 3 2.88 mg/kg		DL 4 4.32 mg/kg		DL 5 6.48 mg/kg		DL 6 9.72 mg/kg	
Parameter	Unit	Mean	STDEV	Mean	STDEV	Mean	STDEV	Mean	STDEV
t1/2	h	54.2	17.34	40.2	16.21	42.2	57.88	20.8	7.74
AUClast	µg/mL*h	5.28	0.92	6.88	0.79	19.2	4.68	153	24
AUCinf	µg/mL*h	5.77	1	7.43	0.97	19.9	6.97	155	25.44
AUCinf/D	µg/L*h/(mg/kg)	2	0.35	1.72	0.23	3.07	1.08	16	2.62
Cl_obs	mL/Kg*h	514	86	596	79.38	343	89.47	64.3	10.52
Vz_obs	L/kg	38.3	6.1	32	9.62	20.6	12.08	1.81	0.4

PK parameter statistics were not calculated for DL 1 and 2, where only one patient was treated. The mean and standard deviation (STDEV) values are shown. t1/2: Terminal half-life; AUClast: Area Under the serum concentration-time Curve within a dosage interval (0 to last measurable concentration) after the first dose; AUCinf: AUC from time of dosing extrapolated to infinity, based on the last predicted concentration; AUCinf/D: AUC from time of dosing extrapolated to infinity, relative to the dose; Cl: Total body clearance; Vz: Volume of distribution based on the terminal phase.

https://doi.org/10.1038/s41591-024-02805-1

Extended Data Table 4 | Detection of Anti-Drug Antibodies (ADAs) in serum over time

Patient ID	Cohort	Dose (mg/kg)	Tumor Type	Screening	C1D8	C1D15	C2D1	C3D1	C4D1	C6D1	C9D1	C12D1	EOT	1 month FU
101-001	1	0.48	CRC	Negative	Negative	Negative	Negative	Negative					Negative	
103-001	2*	1.44	PDAC	Negative	Negative	Negative	Negative	Negative	Negative	Negative**			Negative	Negative
103-002	3	2.88	Meshothelioma	Negative	Negative	Negative	Negative	Negative						Negative
101-002	3*	2.88	PDAC	Negative	Negative	Negative	Negative	Negative	Negative	Negative	Negative		Negative	Negative
102-001	3*	2.88	Salivary Gland	Negative	Negative	Negative	Negative	Negative	Negative***	Negative	102-401			
102-401	4	4.32	Salivary Gland	Negative	Negative	Negative	Negative			Negative	Negative	Negative		
103-003	4	4.32	Sarcoma	Negative	Negative	Negative	Negative	Negative	Negative	Negative	Negative		Negative	Negative
102-002	4	4.32	SCLC	Negative	Negative								Negative	
102-003	4	4.32	PDAC	Negative	Negative	Negative	Negative	Negative					Negative	Negative
101-004	4	4.32	CRC	Negative	Negative	Negative	Negative	Negative					Negative	Negative
102-004	4	4.32	Ovarian	Negative	Negative	Negative	Negative						Negative	
102-006	5	6.48	TNBC	Negative	Negative	Negative	Negative							
103-004	5	6.48	PDAC	Negative	Negative	Negative							Negative	Negative
103-005	5	6.48	PDAC	Negative	Negative	Negative	Negative						Negative	
101-005	5	6.48	NSCLC	Negative	Negative	Negative	Negative	Negative		Negative			Negative	Negative
101-006	5	6.48	CRC	Negative	Negative	Negative	Negative	Negative					Negative	Negative
101-007	5	6.48	CRC	Negative	Negative	Negative	Negative	Negative					Negative	Negative
101-009	5	6.48	CRC	Negative	Negative	Negative	Negative	Negative					Negative	Negative
102-008	5	6.48	PDAC	Negative	Negative	Positive								
103-007	5	6.48	PDAC	Negative	Negative	Negative	Negative						Negative	Negative
102-007	6	9.72	PDAC	Negative	Negative									
103-006	6	9.72	CRC	Negative	Negative	Negative	Negative						Negative	
101-008	6	9.72	CRC	Negative	Negative	Negative	Negative	Negative					Negative	Negative

The presence or absence of ADAs, quantified as positive or negative, at the indicated time points during the OMO-103 Phase I clinical trial is shown. Patient 102-001 ID changed to 102-401 when it was escalated to the next dose level. CRC: colorectal cancer; PDAC: pancreatic ductal adenocarcinoma; SCLC: Small Cell Lung Cancer; TNBC: Triple-Negative Breast Cancer; NSCLC: non-small-cell lung cancer. *Escalated to next dose level; **C6D8; ***C4D15.

https://doi.org/10.1038/s41591-024-02805-1

Extended Data Table 5 | Summary table for all patients and their efficacy results according to RECIST

Patient, N	OMO-103						Total
	0.48 mg/kg (N=1)	1.44 mg/kg (N=1)	2.88 mg/kg (N=3)	4.32 mg/kg (N=5)	6.48 mg/kg (N=9)	9.72 mg/kg (N=3)	(N=22)
Best response							
CR	0	0	0	0	0	0	0
PR	0	0	0	0	0	0	0
SD	0	1	2	2	3	1	9
PD	1	0	1	2	5	1	10
NE*	0	0	0	1	1	1	3

CR complete response; PR partial response; SD stable disease; PD progressive disease; NE not evaluable; *No second assessment. Responses according to RECIST 1.1 by CT scan.

nature portfolio

Corresponding author(s): Laura Soucek

Last updated by author(s): Dec 7, 2023

Reporting Summary

Nature Portfolio wishes to improve the reproducibility of the work that we publish. This form provides structure for consistency and transparency in reporting. For further information on Nature Portfolio policies, see our Editorial Policies and the Editorial Policy Checklist.

Statistics

For all statistical analyses, confirm that the following items are present in the figure legend, table legend, main text, or Methods section.

n/a	Confirmed	
☐	☒	The exact sample size (*n*) for each experimental group/condition, given as a discrete number and unit of measurement
☐	☒	A statement on whether measurements were taken from distinct samples or whether the same sample was measured repeatedly
☐	☒	The statistical test(s) used AND whether they are one- or two-sided *Only common tests should be described solely by name; describe more complex techniques in the Methods section.*
☒	☐	A description of all covariates tested
☐	☒	A description of any assumptions or corrections, such as tests of normality and adjustment for multiple comparisons
☐	☒	A full description of the statistical parameters including central tendency (e.g. means) or other basic estimates (e.g. regression coefficient) AND variation (e.g. standard deviation) or associated estimates of uncertainty (e.g. confidence intervals)
☐	☒	For null hypothesis testing, the test statistic (e.g. *F*, *t*, *r*) with confidence intervals, effect sizes, degrees of freedom and *P* value noted *Give P values as exact values whenever suitable.*
☒	☐	For Bayesian analysis, information on the choice of priors and Markov chain Monte Carlo settings
☒	☐	For hierarchical and complex designs, identification of the appropriate level for tests and full reporting of outcomes
☒	☐	Estimates of effect sizes (e.g. Cohen's *d*, Pearson's *r*), indicating how they were calculated

Our web collection on statistics for biologists contains articles on many of the points above.

Software and code

Policy information about availability of computer code

Data collection	Soluble factors levels were extrapolated from the standard curves using the ProcartaPlex Analyst Software.
Data analysis	DSP data was analyzed using the GeoMxTools R-package (version 3.0.1). Comparisons between groups of patients (stable and progressive disease) were done using the limma R-package (version 3.52.4). Gene Set Enrichment Analysis (GSEA) was conducted using the clusterProfiler R-package (version 4.4.4). Data was plotted using the ggplot2 R-package (version 3.3.6). Soluble factors levels were extrapolated from the standard curves using the ProcartaPlex Analyst Software (version 2.2.0) and plotted using the Graphpad Prism software (version 8). Clinical Statistical analyses were performed by the Clinical Research Organization Simbec-Orion using SAS®, Version 9.4 or later, SAS Institute, Cary, Northern Carolina, USA. The PK analyses were performed from experimental data and using actual sampling times and actual dosing levels of each subject using the PKSolver add-in program for Microsoft Excel by means of a non-compartmental approach. For soluble markers analysis, the Python package Scikit-learn was used to fit the models. Combinations of soluble factors that can correctly stratify patients between PD and SD were found using the QLattice modelling technology (Abzu). Data analysis of OMO-103 quantification from patient biopsies were carried out using SpectroDive™ 11.0 – Biognosys' software for multiplexed PRM data analysis.The DIA mass spectrometric data were analyzed using directDIA+ in Spectronaut software (Biognosys, version 18.4).A human UniProt .fasta database (Homo sapiens, 2023-07-01) was used for the search engine. For volumetric tumor assessment, all those considered measurable by RECIST v1.1 were segmented using the semi-automatic segmentation tool of 3DSlicer (version 4.11.0).

For manuscripts utilizing custom algorithms or software that are central to the research but not yet described in published literature, software must be made available to editors and reviewers. We strongly encourage code deposition in a community repository (e.g. GitHub). See the Nature Portfolio guidelines for submitting code & software for further information.

Data

Policy information about availability of data

All manuscripts must include a data availability statement. This statement should provide the following information, where applicable:

- Accession codes, unique identifiers, or web links for publicly available datasets
- A description of any restrictions on data availability
- For clinical datasets or third party data, please ensure that the statement adheres to our policy

The datasets generated during and/or analysed during the current study used for its analyses are available from the corresponding author on reasonable request. This has been stated in the text.

Human research participants

Policy information about studies involving human research participants and Sex and Gender in Research.

Reporting on sex and gender	This Phase 1 study was open to all patients, regardless of sex, who fulfilled the inclusion criteria. There was also no age limit above 18 years old.
Population characteristics	The study included histologically or cytologically proven advanced solid tumours, for which there was no curative therapy, that had progressed on standard of care (SOC) treatment, were intolerant to it or had no available SOC or for which SOC was unacceptable. Patients had to display measurable disease as per RECIST v1.1 criteria 35 proven by CT/MRI and documented progression on or following the last line of therapy. They also had to present an Eastern Cooperative Oncology Group (ECOG) performance status of up to 1, life expectancy of ≥12 weeks and adequate organ function. Sex was equally distributed between patients; median age was 60.5 years . They were all caucasian and had received between 2 and 12 previous treatments (median 4 treatments).
Recruitment	Patients were selected by very experienced Phase 1 Investigators at 3 sites in Spain; patients had to fulfill all required criteria; ECOG had to be either 0 or 1 and other strict criteria had to be fulfilled (see paragraph above fo details).
Ethics oversight	The study was approved by the ethics committee of the Vall d'Hebron Hospital, Barcelona. However, the final approval for the whole study came from the Spanish "AEMPS". The study was conducted according to the principles of Good Clinical Practice and the Declaration of Helsinki The EC also approved the informed consent form which was used in the clinical trial.

Note that full information on the approval of the study protocol must also be provided in the manuscript.

Field-specific reporting

Please select the one below that is the best fit for your research. If you are not sure, read the appropriate sections before making your selection.

☒ Life sciences ☐ Behavioural & social sciences ☐ Ecological, evolutionary & environmental sciences

For a reference copy of the document with all sections, see nature.com/documents/nr-reporting-summary-flat.pdf

Life sciences study design

All studies must disclose on these points even when the disclosure is negative.

Sample size	As this is a typical Phase 1 study, there is no sample size calculation. An accelerated titration design was used. After the first 2 dose levels with 1 patient each, the 3+3 design was applied, and dose escalation was done until dose level 6.
Data exclusions	As per the safety study, all patients who received the study drug at least once are included into the safety analysis as described in the SAP.
Replication	Not applicable for this Phase 1 study
Randomization	This was a Phase 1 dose escalation study with single agent OMO-103, thus no randomisation was necessary nor applicable.
Blinding	This was a Phase 1 dose escalation study with single agent OMO-103, thus no blinding was necessary nor applicable.

Reporting for specific materials, systems and methods

We require information from authors about some types of materials, experimental systems and methods used in many studies. Here, indicate whether each material, system or method listed is relevant to your study. If you are not sure if a list item applies to your research, read the appropriate section before selecting a response.

Materials & experimental systems

n/a	Involved in the study
☐	☒ Antibodies
☒	☐ Eukaryotic cell lines
☒	☐ Palaeontology and archaeology
☒	☐ Animals and other organisms
☐	☒ Clinical data
☒	☐ Dual use research of concern

Methods

n/a	Involved in the study
☒	☐ ChIP-seq
☒	☐ Flow cytometry
☒	☐ MRI-based neuroimaging

Antibodies

Antibodies used	anti-c-MYC (Y69) Rabbit Monoclonal Primary Antibody (Cat#790-4628) Roche
Validation	INTENDED USE Anti-c-MYC (Y69) Rabbit Monoclonal Primary Antibody is intended for laboratory use in the qualitative immunohistochemical detection of c- MYC protein by light microscopy in sections of formalin-fixed, paraffin- embedded tissue stained on a BenchMark IHC/ ISH instrument. This product should be interpreted by a qualified pathologist in conjunction with histological examination, relevant clinical information, and proper controls. This antibody is intended for in vitro diagnostic (IVD) use.

Clinical data

Policy information about clinical studies

All manuscripts should comply with the ICMJE guidelines for publication of clinical research and a completed CONSORT checklist must be included with all submissions.

Clinical trial registration	NCT04808362; EudraCT No 2020-003802-30
Study protocol	attached as appendix
Data collection	A commercially available eCRF system was used for data collection: Oracle Inform; the access to the system was limited to authorised personnel only. The first patient was enrolled on the May 4th 2021 and the last patient on April 4th 2022;. The recruitment lasted11 months and the last patient came off study January 11th 2023. Site staff entered the data continuously into the system; throughout the study. These entries were controlled by programmed checks of the system but also by the CRAs of the CRO.
Outcomes	Primary endpoint: safety via: • Number of patients with a DLT; • Number of patients with ≥1 related AE; • Number of patients discontinuing study treatment due to related AEs Secondary endpoint: efficacy via CT-imaging according to RECIST eg ORR, PFS, DCR, DOR all AEs and SAEs were collected in the eCRF and later on extracted and evaluated by the statistical team, and methods applied by number, grade and relationship to study drug. Secondary endpoint: efficacy is assessed via pre-planned CT scans, which were evaluated by experienced radiologists according to the well known and validated RECIST criteria. From the responses, several other parameters were derived according to the statistical analysis plan (eg PFS, DCR, DOR). PK was assessed by a specialised laboratory according to the validated method. A specific statistical program was used to analyse the PK data.